

Southward propagation of Nazca subduction along the Andes

Yi-Wei Chen^{1*}, Jonny Wu¹ & John Suppe¹

The Andean margin is the plate–tectonic paradigm for long-lived, continuous subduction, yet its geology since the late Mesozoic era (the past 100 million years or so) has been far from steady state. The episodic deformation and magmatism have been attributed to cyclic changes in the dip angle of the subducting slab, slab break-off and the penetration of the slab into the lower mantle; the role of plate tectonics remains unclear, owing to the extensive subduction of the Nazca–Farallon plate (which has resulted in more than 5,500 kilometres of lithosphere being lost to the mantle). Here, using tomographic data, we recreate the plate–tectonic geometry of the subducted Nazca slab, which enables us to reconstruct Andean plate tectonics since the late Mesozoic. Our model suggests that the current phase of Nazca subduction began at the northern Andes (5° S) during the late Cretaceous period (around 80 million years ago) and propagated southwards, reaching the southern Andes (40° S) by the early Cenozoic era (around 55 million year ago). Thus, contrary to the current paradigm, Nazca subduction has not been fully continuous since the Mesozoic but instead included episodic divergent phases. In addition, we find that foredeep sedimentation and the initiation of Andean compression are both linked to interactions between the Nazca slab and the lower mantle, consistent with previous modelling.

The 7,000-km-long Andean margin (Fig. 1a) is considered the archetypal example of long-lived and monotonous subduction of an oceanic plate beneath a continent^{1–3}. However, the Andean geological record since the early Jurassic period, which is thought to span the most recent period of continuous subduction, shows tectonic signals that are decidedly non-steady-state. Within a presumed context of continuous subduction, episodic and localized deformation, variable magmatic patterns and topographic changes have been attributed to repeated cycles of slab flattening, slab steepening, slab break-off^{4–7} and slab penetration into the lower mantle^{8,9}. The role of margin-wide plate-tectonic events has not been fully explored, owing to the extensive subduction of oceanic lithosphere under western South America, with more than 5,500 km of lithosphere lost since the late Mesozoic 85 million years (Myr) ago.

Tomographic imaging under South America has identified a positive anomaly in P-wave velocity under the Andes that corresponds to an eastward-inclined Nazca slab (Fig. 1). This anomaly follows Benioff-zone seismicity but continues deeper, to depths of around 1,300 km at 8° S and around 1,100 km at 26° S^{10–15} (Figs. 1, 2; Extended Data Figs. 1, 2). The Nazca slab, as referred to here, is a combination of the subducted Farallon plate and the Nazca plate (renamed after the fragmentation of the Farallon plate 23.5 Myr ago). Tomographic images of the Nazca slab^{10–15} are seemingly consistent with a single, long-lived subduction history since the early Jurassic; however, geophysical and geodynamic studies have generally found that the extent of the Nazca slab is insufficient to fully account for the convergence of the Nazca and South American plates since the Cenozoic, let alone that since the Jurassic^{8,14–16} (Extended Data Table 1). Furthermore, below the lowest part of the Nazca slab, at a depth of 1,500 km, two other slab-like anomalies have been identified^{10,14} (Fig. 1b, c; Extended Data Figs. 2, 4). These anomalies imply a more complicated earlier tectonic history, possibly involving a second intra-oceanic subduction zone to the west of South America in the Mesozoic¹⁴.

Geodynamic models have linked the most recent onset of Andean compression to the timing of the penetration of the Nazca slab into

the lower mantle^{8,9}. However, owing to different input plate-tectonic boundary conditions between the two models, these studies predict very different times for when the Nazca slab penetrated the lower mantle: roughly 132 Myr ago⁹ and 50 Myr ago⁸ (Extended Data Table 1). In addition, it is questionable whether the Nazca slab penetrated the lower mantle around either of these times, considering that some studies indicate that Andean subduction began much earlier, during or before the Jurassic¹.

Sedimentological studies have revealed that the southern Andes (south of 35° S) experienced complex episodes of compression and extension^{5,17–19}. These tectonic phases were attributed to changes in the angle of slab dip^{5,17–19}, but we use our plate reconstruction to re-interpret the underlying cause during the Eocene to the Miocene epochs to be interactions between the Nazca slab and the lower mantle.

Here, we aim to reconcile tomography with Andean geology by building a plate model from tomographically imaged subducted lithosphere in the mantle. Our tomographic plate model is relatively independent from Andean geological constraints, which allows us to compare our model implications against geology. Our plate-tectonic reconstruction shows that the latest phase of Andean subduction began at 5° S around 80 Myr ago and propagated southwards to 40° S by about 55 Myr ago. Nazca subduction was not always continuous but was punctuated by episodes of divergence between 80 Myr and 55 Myr ago south of 35° S. Our reconstructed subducted-slab lengths demonstrate that the earliest interactions between the slab and the lower mantle occurred about 10–30 Myr after the onset of Nazca subduction, and these interactions propagate southward. Our tomographic plate model allows images of the mantle structure to be more quantitatively linked to geology and shows promise for other reconstructions of convergent-margin plate tectonics.

Plate tectonics from unfolded slabs

The Nazca slab was mapped in three dimensions from MITP08 P-wave global seismic tomography¹⁰ using the software Gocad. As shown by previous tomographic studies, the Nazca slab widens below a depth of

¹Department of Earth and Atmospheric Sciences, University of Houston, Houston, TX, USA. *e-mail: yiweichen.tw@gmail.com

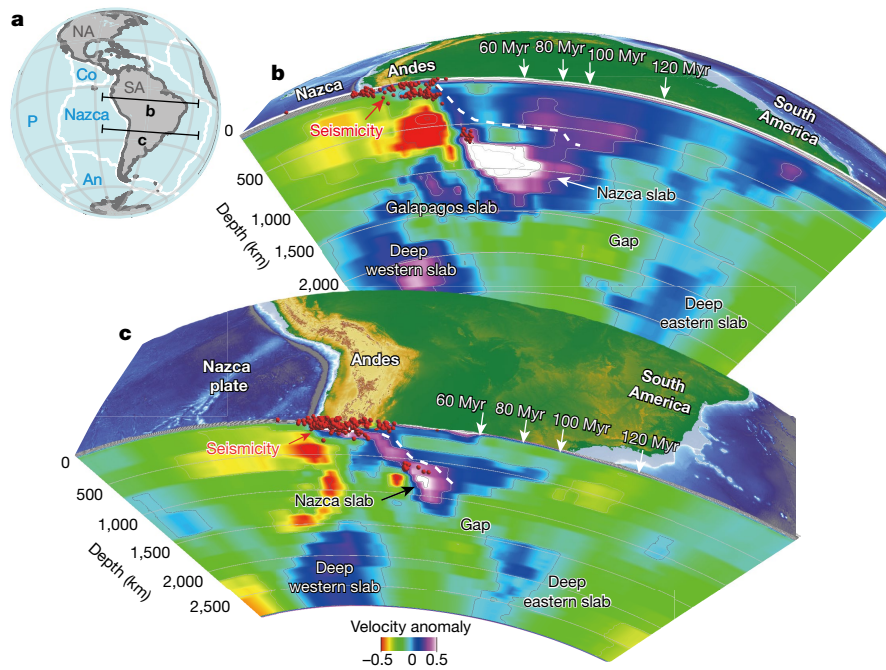


Fig. 1 | Slabs under South America. **a**, Present-day tectonic setting of the southeast Pacific. P, Pacific plate; Co, Cocos plate; An, Antarctica plate; NA, North American plate; SA, South American plate. The Nazca plate is subducting underneath the Andes. **b**, **c**, Tomographic images along the profiles marked in **a** of the subducted Nazca slab from MITP08 tomography¹⁰. The colour scale indicates the perturbation in the P-wave velocity in MITP08. Poorly imaged areas that were delineated by previous

studies are shown as dashed lines^{11–13,15} and are excluded in our analysis. Red dots indicate Benioff-zone seismicity. The reconstructed positions of the Nazca trench³ 120 Myr ago, 100 Myr ago, 80 Myr ago and 60 Myr ago are labelled (see Extended Data Fig. 6 for details). In both profiles, a gap separates the Nazca slab and the deep eastern slab, which we interpret to have resulted from an Andean margin-wide plate reorganization in the late Cretaceous.

600 km, possibly owing to slab folding at a depth of 660 km due to a substantial increase in the viscosity of the mantle^{8,20}. To quantitatively estimate the length of the slab before it subducted and folded (via slab ‘unfolding’), we follow previous work²¹ and measure the area of the slab and incrementally apply a density–depth correction (Methods; Extended Data Fig. 3). Exaggeration of the slab area as a result of tomographic blurring is probable and was considered by comparing a range of arbitrarily reduced slab areas against geological observations (Methods). We assume an initial oceanic lithosphere thickness of about 100 km. Smaller initial lithospheric thicknesses (such as 70 km⁸) are also possible; a smaller value would have the effect of offsetting tomographic blurring (Methods). The Nazca slabs were unfolded across serial cross-sections between 0° S and 40° S (Fig. 3). We did not unfold the Nazca slab south of 40° S owing to image degradation at the southernmost Andes¹⁵. Overall, the unfolded slab lengths decrease from about 7,600 km at 4° S to about 3,800 km at 36° S (Fig. 2a), which together account for roughly 24×10^6 km² of lost oceanic lithosphere (4.7% of Earth’s surface).

We then input our unfolded slab into the palaeo-GIS (geographic information system) GPlates²². We assume that the Nazca slab is still mostly physically attached to the present-day Nazca plate^{10,14} and therefore let the unfolded slab follow the movement of its parent Nazca plate within the plate reconstruction. The motion since 83.5 Myr ago of the Nazca plate relative to the South American plate in our plate model is derived from the global plate circuit and is independent from the reference frame of the mantle. Using the past motion of the Nazca plate from global plate models³, we pull our unfolded Nazca slab out of the mantle under South America (Fig. 3a–d). We find that the leading edge of our unfolded Nazca slab best fits the retro-deformed Andean margin^{23,24} at about 80 Myr ago. This indicates that the tomography of the Nazca slab accounts for the lost lithosphere of the Nazca plate that has been subducting since 80 ± 10 Myr ago, if we consider the error range of the unfolding results (Methods).

Our predicted timing of the initiation of Nazca-slab subduction 80 Myr ago implies a sinking rate into the lower-mantle of

13 ± 4.5 mm yr⁻¹ (Extended Data Fig. 5), which is comparable to the values of 20 ± 8 mm yr⁻¹ determined from geodynamic modelling²⁵ and $(11–12) \pm 3$ mm yr⁻¹ determined from global slab reconstructions^{2,26}. Our time of initiation is also consistent with a comparison of reconstructed positions of the Nazca trench between 100 Myr and 50 Myr ago with the present-day position of the Nazca slab (Extended Data Fig. 6).

We then input our reconstructed Nazca slab into a global plate model³, following a previous method²¹ (Fig. 4). Our tomographic plate model implies that the current phase of Nazca subduction initiated first along the northern Andes (5° S) around 80 Myr ago, and then propagated progressively southwards to 40° S by about 55 Myr ago (Fig. 4; Extended Data Fig. 7; Supplementary Video). Southward shallowing of the base of the Nazca slab in tomography (Fig. 2b), as has been recognized previously⁸, seems to support our prediction based on slab sinking of later subduction initiation at more southern latitudes. During the period when Nazca subduction was limited in the north (80–55 Myr ago), our Nazca slab driven by plate motion³ predicts divergence of the Nazca plate from South America at the southern Andes (Fig. 4; Extended Data Fig. 7). Driving our Nazca slab using an alternative, Antarctic plate circuit²⁷ (Extended Data Fig. 8; see refs^{28,29} for an in-depth discussion) produces similar divergence at the southern Andes. We compare the predictions of our unfolded-slab plate model against geology in section ‘Comparison to Andean geology’.

Interaction between the slab and lower mantle

We use the time-varying subducted-slab lengths predicted by our plate model to estimate the timing of Nazca-slab penetration into the lower mantle (Fig. 5b, green area; Extended Data Fig. 9). From global slab-dip end-members³⁰, we infer that a subducted slab will reach a depth of 660 km (that is, the lower mantle) after 770–1,200 km of slab has been subducted. The two end-members that guide this inference are: the Mariana Pacific slab, which has the shortest length (about 770 km) between the trench and the lower mantle, and the largest

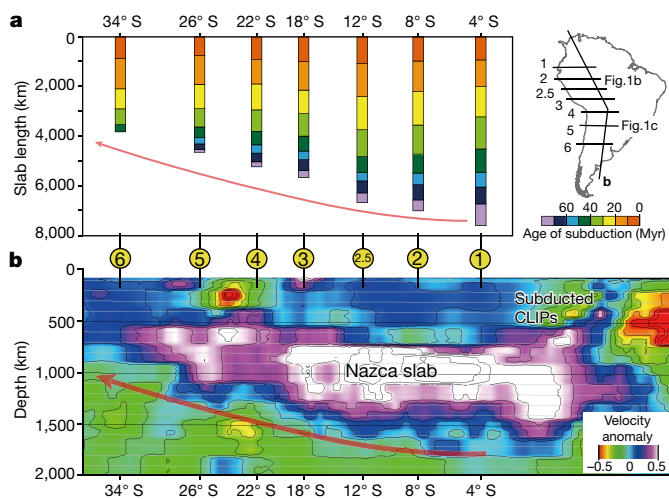


Fig. 2 | Decreasing unfolded Nazca slab lengths and shallowing Nazca slab base towards more southern latitudes. **a**, Unfolded Nazca slab lengths at seven east–west profiles between 4° S and 34° S (see map on the right). **b**, A trench-parallel cross-section from MITP08 tomography, showing intersections with the seven cross-sections from **a**. The subducted Caribbean Large Igneous Province (CLIPs) beneath the Caribbean margin of northwest Columbia is also indicated. Overall, the base of the Nazca slab shallows in the tomography (red arrow in **b**) and the length of the unfolded Nazca slab decreases (red arrow in **a**) towards the south.

dip angle (more than 70°)³⁰; and the Peruvian flat slab, which has a length of about 1,200 km between the trench and the lower mantle and the smallest dip angle (less than 30°)³⁰. Because slab penetration can occur only after the slabs reach 660 km depth, our estimate provides a minimum age for the penetration of the Nazca slab into the lower mantle (Fig. 5b; Extended Data Table 1): roughly 68 Myr ago at northern latitudes (around 6° S) and 35 Myr ago at southern latitudes (around 40° S).

Comparison to Andean geology

The southward propagation of Nazca subduction initiation between 80 Myr and 55 Myr ago that is implied by our plate model (Fig. 5a, red line) is supported by the similar southward propagation of the resumption of Andean-arc magmatism over the same time period (Fig. 5a; see Methods section ‘Magmatism compilation summary’ for a complete list of references). Owing to limited published ages along the southern Andes at about 35° S, magmatic activities at these latitudes shown in

Fig. 5a are inferred from detrital zircon ages³¹. In Extended Data Fig. 10 we provide an alternative comparison of the implications of our model with an independently compiled magmatic catalogue (Extended Data Fig. 10).

Between 80 Myr and 55 Myr ago, our plate-model-driven³ slab reconstruction predicts concurrent subduction at the northern Andes (north of 35° S) and divergence at the southern Andes (south of 35° S) (Fig. 4a–c). The predicted divergence during the late Cretaceous (Fig. 4a) might explain the backarc to intraplate Patagonian basaltic plateaus of Tres Picos Prieto basalts³². The divergence during the Eocene is consistent with previous^{28,33} plate reconstructions of the subduction of the Aluk spreading ridge (Fig. 4c) that led to the eruption of the Eocene Belgrano basalts³³. The reconstructed Aluk ridge seems to correspond to the southern limits of our unfolded Nazca slab (Fig. 4c), which could explain the southern termination of our mapped Nazca slab.

A comparison of our model results to the onset of Andes compression and the development of the foreland basin (Fig. 5b) shows that these events occur progressively more recently to the south, but after our predicted Nazca subduction initiation by 20–30 Myr (Fig. 5b, red line). Other studies have also shown that the onset of Andes compression is decoupled from Nazca subduction rates and lithospheric ages³⁴. On the other hand, Andean compression and foreland basin tectonic signals show similarities to our estimated timing for the Nazca slab reaching the lower mantle (Fig. 5b, green area). These results support previous geodynamic models that have linked the onset of surface compression to lower-mantle slab anchoring^{8,9}. Although we do not make direct predictions for the timing of Nazca-slab anchoring, both the 10–30-Myr delay between our predicted minimum time for the Nazca slab to reach the lower mantle (Fig. 5b, green area) and the onset of Andes compression (Fig. 5b, orange boxes) are consistent with a maximum stagnation time of 60 Myr for slabs to penetrate the lower mantle³⁵.

The southward propagation of Nazca-slab penetration implied by our models (Fig. 5b) would probably have led to a time-transgressive, southward-propagating onset of slab–mantle interactions across the length of the Andes. Our reconstructions of subducted-slab length predict that within the present-day Nazca subduction phase the earliest slab–mantle interactions began at the northern Andes (5° S) about 65 Myr ago and swept southwards to the southern Andes (40° S) by about 30 Myr ago. A key insight from these results is that between 40 Myr and 30 Myr ago at the northern Andes (north of 30° S) there would have been more than 3,000 km of subducted Nazca slab that would have presumably piled up and already anchored into the lower mantle, whereas at the southern Andes (south of 30° S) the Nazca slab was much shorter (about 770 km) and would not be expected to have anchored into the lower mantle (Extended Data Fig. 9). A short and

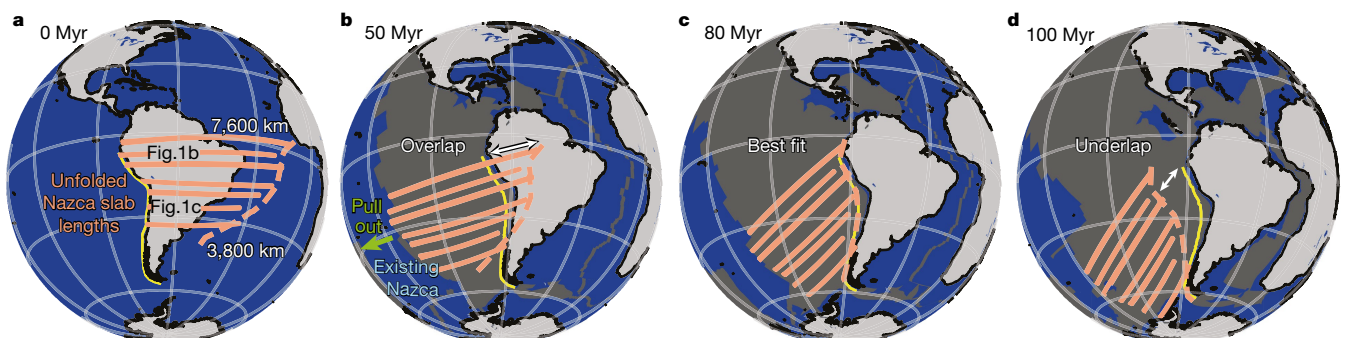


Fig. 3 | Unfolded-slab plate-tectonic reconstruction of Nazca. **a**, The unfolded Nazca slab that is used as the inputs (0 Myr ago) of the global plate-tectonic reconstruction³. The seven orange bars are the unfolded slab lengths of the seven profiles in Fig. 2a. The dashed orange line indicates the leading edge of our unfolded Nazca slab. The yellow line shows the retro-deformed Andean margin^{23,24}. **b–d**, We ‘pull out’ the Nazca slab by attaching it to the Nazca plate and progressively reversing Nazca plate

motions³ in time. Snapshots of the ‘pulled out’ Nazca slab are shown at progressively older times: 50 Myr ago (**b**), 80 Myr ago (**c**) and 100 Myr ago (**d**). Dark grey areas show lithosphere lost owing to subduction. Our unfolded Nazca slab best accounts for lost oceanic lithosphere back to about 80 Myr ago (**c**), which implies that the current phase of Nazca subduction began about 80 Myr ago.

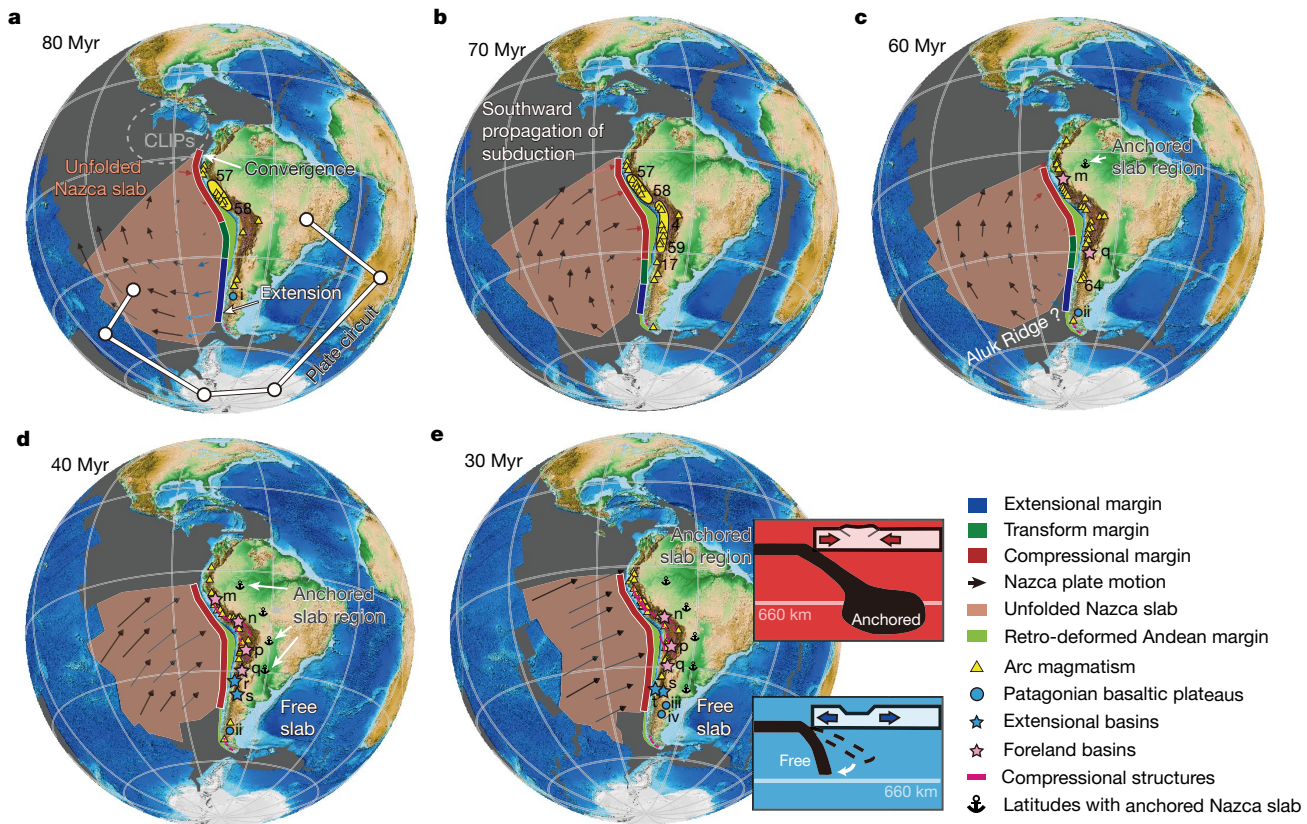


Fig. 4 | Southward propagation of Nazca subduction along the Andes after the late Cretaceous. a–e, Predictions of our plate model 80 Myr (a), 70 Myr (b), 60 Myr (c), 40 Myr (d) and 30 Myr (e) ago (see Extended Data Fig. 7 for details). Arrows indicate the motion of the subducting Nazca plate relative to a fixed South America, which was constrained by plate circuit (see Extended Data Fig. 8 for the motions from the alternative plate circuit). The arrows are colour-coded by the type of plate-tectonic boundary between the Nazca and South American plates: subduction (the compressional margin) is coloured in red; green and blue indicate the transform and divergent (extensional) margins, respectively. The lengths of the arrows indicate relative motion magnitudes. Overall, our model predicts the southward propagation of Nazca subduction. Coloured

symbols denote coeval geological events. Retro-deformed Andean margin (light green) and compressional structures (fuchsia lines) are from ref.²³. Active foreland basins and active extensional basins are shown in pink and blue stars, respectively (m, n, p–t; see Fig. 5 for definitions). Yellow triangles show arc magmatism. The yellow regions highlight the southward propagation of pulses of arc magmatism (see Methods section ‘Magmatism compilation summary’ for references). Blue circles are Patagonian basaltic plateaus (i–iv; see Fig. 5 for definitions). The two insets in e contrast potential differences in slab–mantle interactions between the northern and southern Andes 40 Myr and 30 Myr ago, during which time similar plate convergence conditions existed along the entire Andean margin.

free-moving southern Nazca slab dangling in the upper mantle would be more likely to retreat, creating surface extensional features⁹. This possibly explains the observations of simultaneous northern Andean compression and southern Andean extension between 40 Myr and 20 Myr ago^{5,36–38}, during which time the whole margin was subjected to similar convergence rates (Fig. 4d, e).

Possible Andean evolution before 80 Myr ago

On the basis of the Andean geological record, it was proposed¹ that the latest Andean tectonic cycle started around 190 Myr ago and has continued to the present day without a break. However, we find that the subducted Nazca slab can account for lost lithosphere back to only about 80 Myr ago (Fig. 3); consequently, more slab is necessary to account for subduction and arc magmatism along the Andean margin before 80 Myr ago (Fig. 5a). The two deeper tomographic anomalies (Fig. 1b, c) that lie beneath our Nazca slab are possible candidates, especially the deep eastern anomaly, the position of which is roughly consistent with the reconstructed Andean margin 100 Myr ago (Fig. 1c; Extended Data Fig. 6). Because the slab anomaly extends down to the core–mantle boundary, it could account for the continuous subduction at the Andes between 80 Myr and roughly 200 Myr ago, given our calculated slab sinking rates ($13 \pm 4.5 \text{ mm yr}^{-1}$). In this case, there is enough slab within the mantle to account for subduction over the whole 190-Myr Andean tectonic cycle.

The deeper slab anomalies are separated from the Nazca slab by an obvious and continuous slab gap at a depth of $1,500 \pm 150 \text{ km}$ (Fig. 1; Extended Data Fig. 2). Our results suggest that this gap resulted from a substantial reorganization in subduction of the Nazca plate sometime before 80 Myr ago, during the 190-Myr Andean tectonic cycle (Fig. 5a). We cannot exclude the possibility that this slab gap was produced by the sinking of a once-continuous Nazca and deep eastern slab, which then broke apart in the mantle and sank at different rates. However, our interpretation is compatible with previous studies that show a substantial, margin-wide change between 100 Myr and 80 Myr ago, such as a margin-wide compressional event³⁹, the closure of marginal basins^{40,41}, the formation of foreland basins^{17,42}, a change in strike-slip fault motions⁴³ or a marked change in geochemical signals from 100 Myr to 80 Myr ago⁴⁴.

The Andean margin-wide reorganization 100–80 Myr ago has previously been attributed to incremental westward drift of South America^{18,45,46}, but this westward drift is not robustly reproduced within alternative mantle reference frames (Extended Data Fig. 6). For example, plate reconstructions in the ‘hybrid’ and ‘slab’ mantle reference frames show only minor (0–350 km) absolute westward drift of South America between 100 Myr and 80 Myr ago³ (Extended Data Fig. 6). Because our study is not sensitive to different mantle reference frames, it provides an alternative explanation for how this margin-wide event might be linked to a plate-tectonic reorganization.

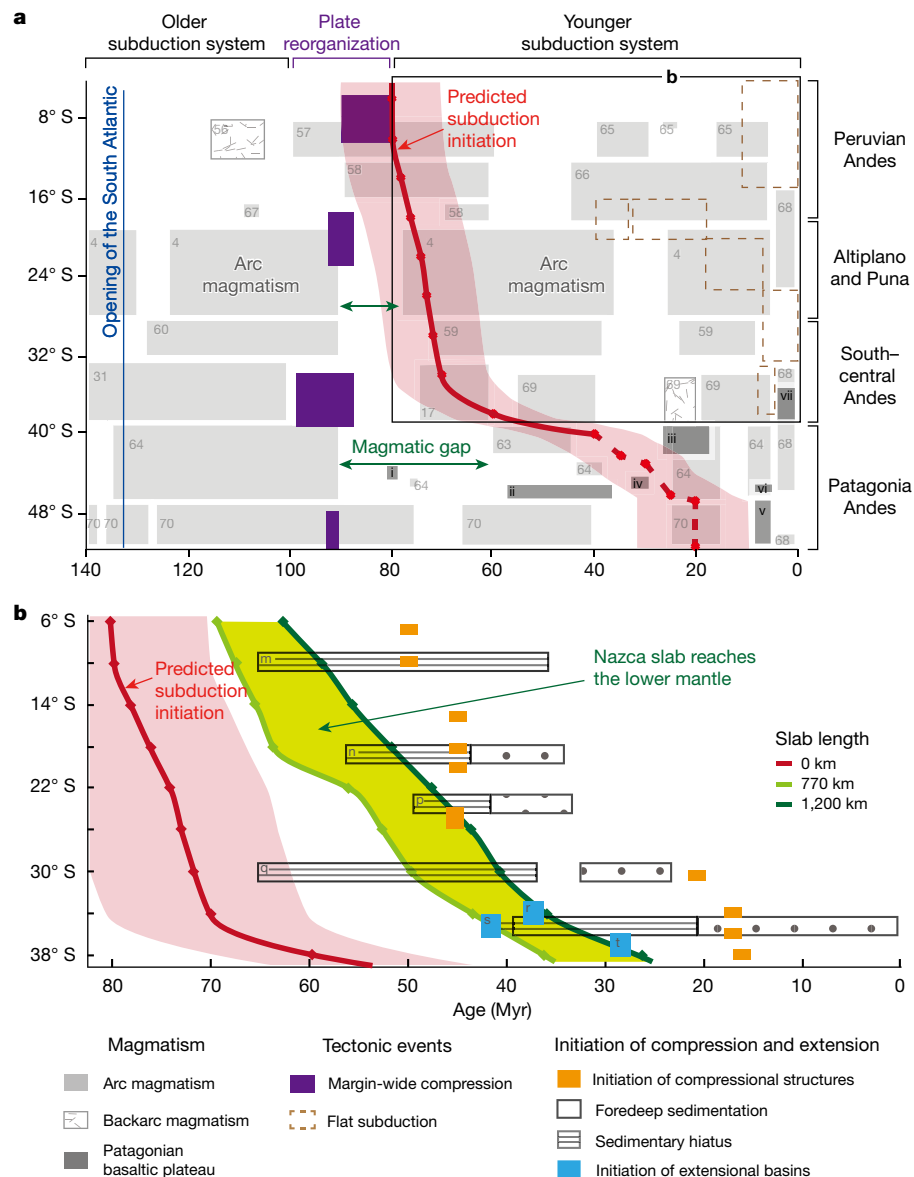


Fig. 5 | Comparison of plate-model predictions with Andean geology. **a**, The onset of Nazca subduction and a comparison with Andean magmatism. Our proposed 140-Myr-long Andean evolution is labelled at the top. The thick red line highlights the southward propagation of the initiation of Nazca subduction predicted by our plate model, at the latitudes shown by the red dots. Model predictions within the less-well-imaged area (south of 40° S) are shown by a red dashed line. The error range (± 10 Myr; red shaded area) comes from alternative choices of slab-edge velocity perturbations (Methods). Purple rectangles show the Andean margin-wide compressional event in the late Cretaceous³⁹. Light grey rectangles show arc-related magmatism and striped rectangles show backarc magmatism (see Methods for details and references). The green arrows highlight the magmatic gap that occurred before the predicted Nazca subduction initiation. Dark grey rectangles are Patagonian basaltic plateaus^{33,52}: i, Tres Picos Prieto basalts; ii, Belgrano basalts; iii, Somuncura basalts; iv, Kankel basalts; v, Meseta de la Muerte basalts; vi, Pico Truncado basalts; vii, Payenia basalts. Brown dashed boxes show previously

proposed flat subduction events⁶. **b**, Our reconstructed subducted Nazca slab lengths as a function of latitude and time. The red line and shading shows the initiation of Nazca subduction, as in **a** (along this line the slab length is 0 km). The light green and dark green lines show the times at which subducted Nazca slab lengths reached 770 km (Mariana-like) and 1,200 km (Peru-like), respectively. The lime green area between the two green lines indicates our inferred minimum time range for the subducted Nazca slab to reach the lower mantle (which lies at a depth of 660 km), at each latitude. Geological evidence for the initiation of compressional structures is represented by orange rectangles (see ref.⁸ and references therein and ref.²³). The timing of foredeep deposits (dotted areas) and foreland basin unconformities that indicate a sedimentary hiatus (hashed areas) are also shown¹⁸: m, Cordillera Blanca; n, eastern Cordillera; p, Cordillera Oriental; q, Bermejo. The onset of extensional basins is represented by blue rectangles: r, Abanico basin³⁷; s, Neuquén basin¹⁷; t, Loncopué trough³⁸ and Cura-Mallín basin³⁶.

Published global plate models do not implement a margin-wide plate reorganization along the Andes before 80 Myr ago³, but Nazca plate kinematics during this period are less well constrained owing to the lack of a plate circuit before 83.5 Myr ago³. Furthermore, the deep western anomaly in the lower mantle¹⁴ (Fig. 1b, c) seems to imply an intra-oceanic subduction zone approximately 2,000 km west of western South America sometime between 200 Myr and 80 Myr ago. Intra-oceanic subduction zones have also been proposed further north along western

North America during the Cretaceous⁴⁷. These and other plate reconstruction complexities (such as the conceptual Chasca and Catequil plates²⁷) could allow the plate reconstruction details presented here to fit within the constraints of current plate models³, at least near the southern Gondwana margin. Further study is needed to understand the regional context for our proposed reorganization at the Andes, and its possible roles and relationships with adjacent plate reorganizations at the southern Gondwana margin 105–100 Myr ago⁴⁸.

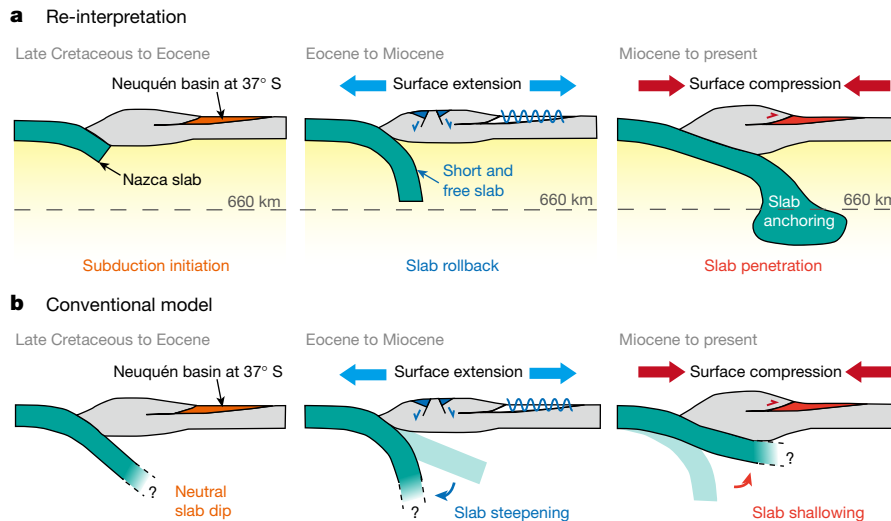


Fig. 6 | Re-interpreted tectonic evolution of the Neuquén basin at 37° S. **a, b,** Different interpretations of the evolution of the Neuquén basin at the late Cretaceous to Eocene (left), Eocene to Miocene (middle) and Miocene to present (right). Blue and red arrows highlight surface extension and compression, respectively. Wavy blue lines show the timing of unconformities in the Neuquén basin from sedimentary records^{5,17}. **a,** Re-interpretation based on our plate model. Initiation of Nazca subduction in the late Cretaceous is followed by interactions between the slab and the lower mantle. The top of the lower mantle (660 km depth) is by the

black dashed line. From the Eocene to the Miocene, our model predicts a short and free-moving upper-mantle slab that allows slab retreat and the formation of extensional basins. During the Miocene, the Nazca slab anchored into the lower mantle, producing compression. **b,** Conventional flat-slab model^{5,17}, showing multiple changes in the dip angle of the Nazca slab. Steepening of the Nazca slab in the Eocene and shallowing in the Miocene (to yield a flat slab) are invoked to explain an extensional episode followed by a compressive episode in the Neuquén basin^{5,17}.

Differentiating plate tectonics from flat slabs

Our proposed Andean tomographic plate reconstruction provides insights into the roles of margin-wide plate-tectonic reorganizations and slab–mantle interactions relative to other factors (flat-slab subduction or slab break-off) since the late Mesozoic. We propose that a new subduction system—the present-day Nazca subduction phase—initiated along the northern Andes (5° S) about 80 Myr ago and propagated to the southern Andes (40° S) by 55 Myr ago. Our model shows that southward-propagating Nazca subduction initiation and later lower-mantle Nazca slab anchoring has also influenced the first-order evolution of the Andes.

Between the late Cretaceous and the Eocene (Fig. 4a–c), the southward propagation of Nazca subduction controlled the first-order evolution of the Andes, producing southward propagation of subduction-related arc magmatism (Fig. 5a). Traditionally, a new magmatic pulse following a magmatic lull has been linked to flat-slab subduction^{4,49–51}; however, areas affected by flat-slab subduction are usually localized (see ref. 6 for a review). The margin-wide, southward-propagating initiation of Nazca subduction predicted by our model can better explain the systematic change that is observed in Andean magmatism (Fig. 5a).

From the Eocene to the Miocene (Fig. 4d, e), the entire Andean margin finally became a subduction margin, with similar convergence rates across the entire margin (Fig. 4d, e). The differences in our reconstructed subducted-slab lengths during this period imply contrasting slab–mantle interactions which potentially explain the tectonic differences across the Andes (Fig. 4e). Specifically, during this phase, the longer northern Nazca slab penetrated into the lower mantle whereas the shorter southern Nazca slab probably remained free within the upper mantle or transition zone (Fig. 4e, insets). This is notable because previous modelling studies (for example, ref. 9) have shown that anchored lower-mantle slabs promote compressional structures whereas non-anchored slabs allow trench retreat and produce extensional structures.

For each area of the Andes, a transition from a short and free upper-mantle slab to an anchored lower-mantle slab should occur. The sedimentary records for the well-studied Neuquén basin show a complex history that consists of an early (about 100 Myr ago) compressional

phase, followed by neutral subduction, then Eocene extension and finally Miocene compression¹⁷ (Fig. 6). The complex tectonic history has been interpreted within the context of complex changes in slab dip angle^{5,17} (Fig. 6b). Our Nazca slab length reconstruction allows us to reinterpret the tectonic history of the Neuquén basin to show that after Nazca subduction initiated about 80 Myr ago the Nazca slab remained short and free, allowing retreat and extensional basins to form. It is not until later (around the Miocene) that subducted-slab lengths were sufficient to permit possible slab penetration into the lower mantle, producing structural inversion (Fig. 6). Therefore, we suggest that the Neuquén basin sediments actually reflect a natural and expected tectonic evolutionary sequence after the initiation of Nazca subduction—changes in slab dip are not required.

It is only since the Miocene that our plate model implies a single and continuous Nazca subduction regime that is reminiscent of the classical Andean model. By excluding plate tectonic phenomena, our model implies that Andean tectonics was dominated by flat slabs during this period, supporting the popular Andean paradigm⁶ from the Miocene to the present day.

Online content

Any methods, additional references, Nature Research reporting summaries, source data, statements of data availability and associated accession codes are available at <https://doi.org/10.1038/s41586-018-0860-1>.

Received: 10 April 2018; Accepted: 20 November 2018;

Published online 23 January 2019.

1. Mpodozis, C. & Ramos, V. in *Geology of the Andes and its Relation to Hydrocarbon and Mineral Resources* (eds Ericksen, G. E., Cañas Pinochet, M. T. & Reinemud, J. A.) 59–90 (Circum-Pacific Council for Energy and Mineral Resources, 1989).
2. van der Meer, D. G., Spakman, W., Van Hinsbergen, D. J., Amaru, M. L. & Torsvik, T. H. Towards absolute plate motions constrained by lower-mantle slab remnants. *Nat. Geosci.* **3**, 36–40 (2010).
3. Müller, R. D. et al. Ocean basin evolution and global-scale plate reorganization events since Pangea breakup. *Annu. Rev. Earth Planet. Sci.* **44**, 107–138 (2016).
4. Haschke, M. R., Scheuber, E., Günther, A. & Reutter, K. J. Evolutionary cycles during the Andean orogeny: repeated slab breakoff and flat subduction? *Terra Nova* **14**, 49–55 (2002).
5. Horton, B. K. & Fuentes, F. Sedimentary record of plate coupling and decoupling during growth of the Andes. *Geology* **44**, 647–650 (2016).

6. Ramos, V. A. & Folguera, A. Andean flat-slab subduction through time. *Geol. Soc. Lond. Spec. Publ.* **327**, 31–54 (2009).
7. Ramos, V. A. & Kay, S. M. in *Evolution of an Andean Margin: A Tectonic and Magmatic View from the Andes to the Neuquén Basin (35°–39°S lat)* (eds Kay, S. M. & Ramos, V. A.) 1–18 (Geological Society of America, Boulder, 2006).
8. Faccenna, C., Oncken, O., Holt, A. F. & Becker, T. W. Initiation of the Andean orogeny by lower mantle subduction. *Earth Planet. Sci. Lett.* **463**, 189–201 (2017).
9. Schellart, W. P. Andean mountain building and magmatic arc migration driven by subduction-induced whole mantle flow. *Nat. Commun.* **8**, 2010 (2017).
10. Li, C., van der Hilst, R. D., Engdahl, E. R. & Burdick, S. A new global model for P wave speed variations in Earth's mantle. *Geochem. Geophys. Geosyst.* **9**, Q05018 (2008).
11. Scire, A., Zandt, G., Beck, S., Long, M. & Wagner, L. The deforming Nazca slab in the mantle transition zone and lower mantle: constraints from teleseismic tomography on the deeply subducted slab between 6°S and 32°S. *Geosphere* **13**, 665–680 (2017).
12. Scire, A., Biryol, C. B., Zandt, G. & Beck, S. Imaging the Nazca slab and surrounding mantle to 700 km depth beneath the central Andes (18°S to 28°S). *Geol. Soc. Am.* **212**, 23–41 (2014).
13. Scire, A. et al. Imaging the transition from flat to normal subduction: variations in the structure of the Nazca slab and upper mantle under southern Peru and northwestern Bolivia. *Geophys. J. Int.* **204**, 457–479 (2016).
14. Grand, S. P. Mantle shear structure beneath the Americas and surrounding oceans. *J. Geophys. Res. Solid Earth* **99**, 11591–11621 (1994).
15. Ren, Y., Stutzmann, E., van Der Hilst, R. D. & Besse, J. Understanding seismic heterogeneities in the lower mantle beneath the Americas from seismic tomography and plate tectonic history. *J. Geophys. Res. Solid Earth* **112**, B01302 (2007).
16. Quinteros, J. & Sobolev, S. V. Why has the Nazca plate slowed since the Neogene? *Geology* **41**, 31–34 (2013).
17. Horton, B. K. et al. Andean stratigraphic record of the transition from backarc extension to orogenic shortening: a case study from the northern Neuquén basin, Argentina. *J. S. Am. Earth Sci.* **71**, 17–40 (2016).
18. Horton, B. K. Sedimentary record of Andean mountain building. *Earth Sci. Rev.* **178**, 279–309 (2018).
19. Horton, B. K. Tectonic regimes of the central and southern Andes: responses to variations in plate coupling during subduction. *Tectonics* **37**, 402–429 (2018).
20. Ribe, N. M., Stutzmann, E., Ren, Y. & van der Hilst, R. Buckling instabilities of subducted lithosphere beneath the transition zone. *Earth Planet. Sci. Lett.* **254**, 173–179 (2007).
21. Wu, J., Suppe, J., Lu, R. & Kanda, R. Philippine Sea and East Asian plate tectonics since 52 Ma constrained by new subducted slab reconstruction methods. *J. Geophys. Res. Solid Earth* **121**, 4670–4741 (2016).
22. Boyden, J. A. et al. in *Geoinformatics: Cyberinfrastructure for the Solid Earth Sciences* (eds Baru, C. & Keller, G. R.) 95–114 (Cambridge Univ. Press, Cambridge, 2011).
23. Schepers, G. et al. South-American plate advance and forced Andean trench retreat as drivers for transient flat subduction episodes. *Nat. Commun.* **8**, 15249 (2017).
24. McQuarrie, N. Initial plate geometry, shortening variations, and evolution of the Bolivian orocline. *Geology* **30**, 867–870 (2002).
25. Steinberger, B., Torsvik, T. H. & Becker, T. W. Subduction to the lower mantle – a comparison between geodynamic and tomographic models. *Solid Earth* **3**, 415–432 (2012).
26. Shephard, G. E., Matthews, K. J., Hosseini, K. & Domeier, M. On the consistency of seismically imaged lower mantle slabs. *Sci. Rep.* **7**, 10976 (2017).
27. Seton, M. et al. Global continental and ocean basin reconstructions since 200 Ma. *Earth Sci. Rev.* **113**, 212–270 (2012).
28. Wright, N. M., Seton, M., Williams, S. E. & Müller, R. D. The late Cretaceous to recent tectonic history of the Pacific Ocean basin. *Earth Sci. Rev.* **154**, 138–173 (2016).
29. Matthews, K. J. et al. Geologic and kinematic constraints on late Cretaceous to mid Eocene plate boundaries in the southwest Pacific. *Earth Sci. Rev.* **140**, 72–107 (2015).
30. Lallemand, S., Heuret, A. & Boutelier, D. On the relationships between slab dip, back-arc stress, upper plate absolute motion, and crustal nature in subduction zones. *Geochem. Geophys. Geosyst.* **6**, Q09006 (2005).
31. Fennell, L. M. et al. Cretaceous deformation of the southern central Andes: synorogenic growth strata in the Neuquén Group (35° 30'–37° S). *Basin Res.* **29**, 51–72 (2015).
32. Zaffarana, C. B., Lagorio, S. L. & Somoza, R. Paleomagnetism and geochemistry from the Upper Cretaceous Tres Picos Prieto locality (43°S), Patagonian plateau basalts. *Andean Geol.* **39**, 53–66 (2012).
33. Kay, S. M., Gorring, M. & Ramos, V. A. Magmatic sources, setting and causes of Eocene to recent Patagonian plateau magmatism (36°S to 52°S latitude). *Rev. Asoc. Geol. Argent.* **59**, 556–568 (2004).
34. Maloney, K. T., Clarke, G. L., Klepeis, K. A. & Quevedo, L. The Late Jurassic to present evolution of the Andean margin: drivers and the geological record. *Tectonics* **32**, 1049–1065 (2013).
35. Goes, S., Agrusta, R., van Hunen, J. & Garel, F. Subduction-transition zone interaction: a review. *Geosphere* **13**, 644–664 (2017).
36. Burns, W. M., Jordan, T. E., Copeland, P. & Kelley, S. A. The case for extensional tectonics in the Oligocene-Miocene southern Andes as recorded in the Cura Mallín basin (36–38 S). *Geol. Soc. Am. Spec. Pap.* **407**, 163–184 (2006).
37. Charrier, R. et al. Evidence for Cenozoic extensional basin development and tectonic inversion south of the flat-slab segment, southern Central Andes, Chile (33–36 SL). *J. S. Am. Earth Sci.* **15**, 117–139 (2002).
38. Folguera, A., Rojas Vera, E., Bottesi, G., Zamora Valcarce, G. & Ramos, V. A. The Loncopué trough: a Cenozoic basin produced by extension in the southern Central Andes. *J. Geodyn.* **49**, 287–295 (2010).
39. Tunik, M., Folguera, A., Naipauer, M., Pimentel, M. & Ramos, V. A. Early uplift and orogenic deformation in the Neuquén basin: constraints on the Andean uplift from U–Pb and Hf isotopic data of detrital zircons. *Tectonophysics* **489**, 258–273 (2010).
40. Pfiffner, O. & Gonzalez, L. Mesozoic–Cenozoic evolution of the western margin of South America: case study of the Peruvian Andes. *Geosciences* **3**, 262–310 (2013).
41. Poblete, F. et al. Late Cretaceous–early Eocene counterclockwise rotation of the Fuegian Andes and evolution of the Patagonia–Antarctic Peninsula system. *Tectonophysics* **668–669**, 15–34 (2016).
42. Bascuñán, S., Arriagada, C., Le Roux, J. & Deckart, K. Unraveling the Peruvian phase of the central Andes: stratigraphy, sedimentology and geochronology of the Salar de Atacama basin (22°30'–23°S), northern Chile. *Basin Res.* **28**, 365–392 (2016).
43. Hoffmann-Rothe, A. et al. in *The Andes: Active Subduction Orogeny* (eds Oncken, O. et al.) 125–146 (Springer, Berlin, 2006).
44. Haschke, M. et al. in *The Andes: Active Subduction Orogeny* (eds Oncken, O. et al.) 337–353 (Springer, Berlin, 2006).
45. Somoza, R. & Zaffarana, C. B. Mid-Cretaceous polar standstill of South America, motion of the Atlantic hotspots and the birth of the Andean cordillera. *Earth Planet. Sci. Lett.* **271**, 267–277 (2008).
46. Ramos, V. A. Anatomy and global context of the Andes: main geologic features and the Andean orogenic cycle. *Geol. Soc. Am.* **204**, 31–65 (2009).
47. Sigloch, K. & Mihalynuk, M. G. Intra-oceanic subduction shaped the assembly of Cordilleran North America. *Nature* **496**, 50–56 (2013).
48. Matthews, K. J., Seton, M. & Müller, R. D. A global-scale plate reorganization event at 105–100 Ma. *Earth Planet. Sci. Lett.* **355–356**, 283–298 (2012).
49. Folguera, A. et al. A review of late Cretaceous to Quaternary palaeogeography of the southern Andes. *Biol. J. Linn. Soc.* **103**, 250–268 (2011).
50. Ramos, V. A. & Folguera, A. Tectonic evolution of the Andes of Neuquén: constraints derived from the magmatic arc and foreland deformation. *Geol. Soc. Lond. Spec. Publ.* **252**, 15–35 (2005).
51. Parada, M. A. et al. Mesozoic and Cenozoic plutonic development in the Andes of central Chile (30°30'–32°30'S). *J. S. Am. Earth Sci.* **1**, 249–260 (1988).
52. Folguera, A. et al. Retroarc volcanism in the northern San Rafael Block (34°–35°30'S), southern Central Andes: occurrence, age, and tectonic setting. *J. Volcanol. Geotherm. Res.* **186**, 169–185 (2009).

Acknowledgements Y.-W.C. and J.W. acknowledge support from University of Houston funds. J.S. acknowledges funding from Texas Governor's University Research Initiative funds (GURI) and the University of Houston. Educational licences for the software Gocad were provided by Paradigm through the Paradigm University Program. We thank J. Saylor, B. K. Horton, C. Faccenna, S. M. Kay and M. Riesner for discussions.

Reviewer information Nature thanks D. Muller and the other anonymous reviewer(s) for their contribution to the peer review of this work.

Author contributions J.W. conceived and designed the study. Y.-W.C. generated the plate model and synthesized the Andean geology. Y.-W.C. and J.W. wrote the manuscript. Y.-W.C., J.W. and J.S. developed the tectonic arguments.

Competing interests The authors declare no competing interests.

Additional information

Extended data is available for this paper at <https://doi.org/10.1038/s41586-018-0860-1>.

Supplementary information is available for this paper at <https://doi.org/10.1038/s41586-018-0860-1>.

Reprints and permissions information is available at <http://www.nature.com/reprints>.

Correspondence and requests for materials should be addressed to Y.-W.C. **Publisher's note:** Springer Nature remains neutral with regard to jurisdictional claims in published maps and institutional affiliations.

METHODS

Slab unfolding. To unfold the slab, we first mapped the fast anomaly in three dimensions. This step helps us to exclude tomographic artefacts or other slabs that are in contact with the Nazca slab (Fig. 1b). We then cut various east–west spherical-Earth tomographic cross-sections. On each cross-section, we picked the steepest velocity-perturbation gradient as the edge of the Nazca slab. This criterion works well in most cases, except at larger depths where the velocity gradient decreases, possibly owing to the reduction of ray path coverage. For example, in Extended Data Fig. 3c the edge of the Nazca slab can easily be selected from the steepest velocity-perturbation gradient around the anomaly, except in the deeper eastern part between 900 km and 1,300 km, where the fast anomaly gradually fades into the ambient mantle (Extended Data Fig. 3). In these cases, we picked velocity perturbations ($dV_p = +0.3\%$ and $+0.2\%$) that have been suggested⁵³ to be the most likely for a slab edge. We correct for slab density–depth changes using the PREM Earth model⁵⁴.

Similarly to previous work¹⁵, we assume that a reasonable pre-subduction thickness of the oceanic lithosphere is about 100 km, on the basis of synthetic lithospheric age models³. Smaller initial thicknesses (such as 70 km)¹⁴ are also possible. The choice of a smaller value would increase the unfolded slab lengths (green dots in Extended Data Fig. 10) and have the effect of counteracting tomographic blurring artefacts (considered below). We then obtain two possible slab lengths, with a maximum of 8,188 km (when using $dV_p = +0.2\%$ to define the slab edge) and a minimum of 6,694 km (when using $dV_p = +0.3\%$ to define the slab edge). From the Nazca–South America convergence rate³, we derive the subducted ages from subducted-slab lengths (Extended Data Fig. 3d), obtaining a maximum of 90 Myr and a minimum of 70 Myr. Thus, the anomaly accounts for subducted lithosphere back to sometime between 90 Myr and 70 Myr ago. We then took the middle value (80 Myr), with a possible age range of ± 10 Myr. The results of all of the measurements on different cross-sections are listed in Fig. 3. Overall, the restored slab length decreases from north to south, and the subducted ages are younger towards the south (Extended Data Table 1).

Differences in Nazca slab lengths estimated by other studies^{8,15} might come from the resolution of different topographies, differences in assumed initial slab lithospheric thicknesses (100 km or 70 km), and different selected velocity perturbations for the slab edge (0.25%–0.5%). Our unfolded slab lengths are generally longer (by about 20%) compared to previous measurements at the same location. This is probably because our unfolding procedure following ref. ²¹ includes a correction for the density increment, which usually increases the slab area by 15%–35%.

Unfolding the Nazca slab from other tomographies does not result in very different unfolded slab lengths (Extended Data Fig. 4). However, tomographic blurring necessarily exists and would exaggerate our estimated slab areas. To assess these tomographic uncertainties, we first compared input and recovered slab volumes from a synthetic Nazca slab resolution test for MITP08 tomography of the upper 660 km along a northeast–southwest cross-section at about 18° S⁵⁵. The test showed 6% exaggeration of the input slab area due to tomographic blurring⁵⁵. However, considering that this is the only relevant test in our study area and the recovered image is only available within the upper 660 km, the robustness of imaged slab areas remains unknown, especially in the lower mantle, where we observed possibly buckled slabs (Fig. 1). Checkerboard resolution tests show overall good recovery underneath South America at various depths¹⁰; however, given the checkerboard spacing of about 550 km in the upper mantle and of about 600 km in the lower mantle¹⁰, the tomographic resolution is probably closer to several hundred kilometres rather than the stated 100-km maximum¹⁰. Therefore, it is possible that the wider slab anomalies in the lower mantle have been exaggerated as a result of tomographic blurring. Therefore, slab areas might be overestimated. We considered the possible effects of tomographic blurring by arbitrarily shrinking our unfolded slab lengths by 20% and 40% and comparing the plate-model outcomes against magmatism (Extended Data Fig. 10). For all cases, southward-propagating Nazca subduction was preserved, but timings and implied slab sinking rates were altered (Extended Data Fig. 10a). The plate model with 80% of our preferred slab lengths showed later initiation of Nazca subduction, from about 65 Myr ago at 8° S to 30 Myr ago at 40° S. The implied lower-mantle sinking rate was about 17 mm yr⁻¹. The 60% slab length model showed subduction initiation about 50 Myr ago at 8° S and 25 Myr ago at 40° S; a lower-mantle sinking rate of around 27 mm yr⁻¹ was produced. Shorter slab lengths were not tested because they would have produced unreasonably fast slab sinking rates. The 80% and 60% slab length models compare less well to the geology, the magmatism and the plate reorganization 100–80 Myr ago (Fig. 5a, Extended Data Fig. 10). Therefore, we conclude that the true slab lengths are unlikely to be smaller than 80% of our preferred slab lengths.

Slab sinking rate calculations. Following a previous approach²¹, we used the Nazca slab age–depth relationship to obtain a slab sinking rate. The Nazca slab subduction age was derived by graphically inspecting the time at which the reconstructed Nazca plate overlapped the western South American margin within our

plate reconstruction. The slab depth was obtained directly from tomographic cross-sections. Sinking rates were then estimated by regressing the slab subduction ages and slab depths (Extended Data Fig. 5).

Magmatism compilation summary. As with any region, the Andean magmatic record is not fully complete owing to sampling, erosion and possibly subduction erosion, but it provides a quantitative assessment of Andean subduction history for comparison to our study. In Fig. 5a, we show the tectonic origin of each magmatic record inferred from published geochemical signatures (in terms of arc, backarc or intraplate magmatism). This provides a feature-by-feature comparison between magmatism sourced from similar tectonic settings. In northern Peru (8°–12° S), the marginal-basin deposits of the Casma group⁵⁶ was intruded by the 102–59-Myr-old arc-like coastal batholith⁵⁷, indicating the start of subduction around 100 Myr ago. In southern Peru (16°–17° S), arc-like magmatism resumed abruptly 90 Myr ago after a magmatic gap that began in the Jurassic⁵⁸. In northern Chile (21°–26° S), four magmatic episodes have been proposed⁴, including an arc resumption at the Chilean Precordillera 78 Myr ago. In central Chile (30°–32° S), the arc magmatism at the Principal Cordillera of Chile resumed 72.6 Myr ago⁵⁹ after a magmatic gap⁵¹. In southern–central Chile (36°–38° S), the onset and duration of the early magmatic episodes are poorly constrained⁶⁰, because pre-Cenozoic magmatic rock exposures are limited. As a result, our understanding of magmatism at these latitudes comes from the ages of detrital zircons in sedimentary basins. The absence of mid- to late-Cretaceous zircons^{17,31,39,61} led to an interpretation³¹ of arc waning after around 100 Myr ago, whereas the dominance of zircons 75–60 Myr ago indicates substantial contributions from a coeval magmatic arc¹⁷. We therefore took 75 Myr ago as the time for arc resumption, although a few older K–Ar ages have been reported⁶². Further south in Chile and Argentina (39°–43° S), the Pilcaniyeu volcanic belt resumed around 60 Myr ago⁶³. At the north Patagonian Andes (44°–47° S), the main plutonic pulses ceased 90 Myr ago and resumed 25 Myr ago, with geographically limited eruptions 75 Myr and 40 Myr ago⁶⁴.

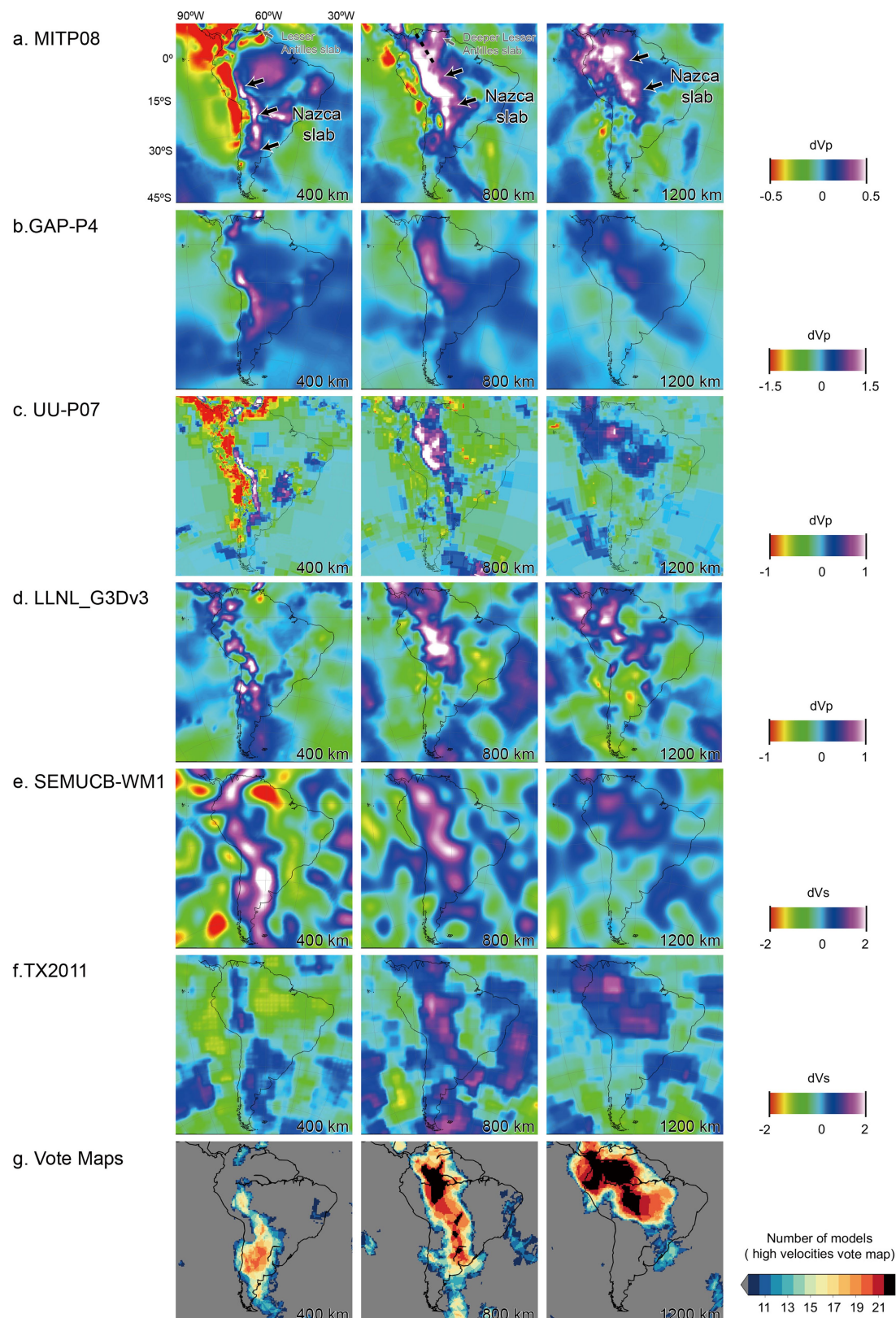
The other arc magmatic pulses in Fig. 5a are compiled from refs. ^{4,17,31,51,57,58,63–70}. To provide an alternative perspective, we also plotted an undifferentiated Andean magmatic catalogue⁷¹, which contains more than 14,000 records, to compare against the predictions of our plate model (Extended Data Fig. 10). Extended Data Fig. 10 offers a complementary perspective on Fig. 5a by providing an independent view of magmatic histories against our model predictions.

Data availability

The data that support the findings of this study are available within the paper.

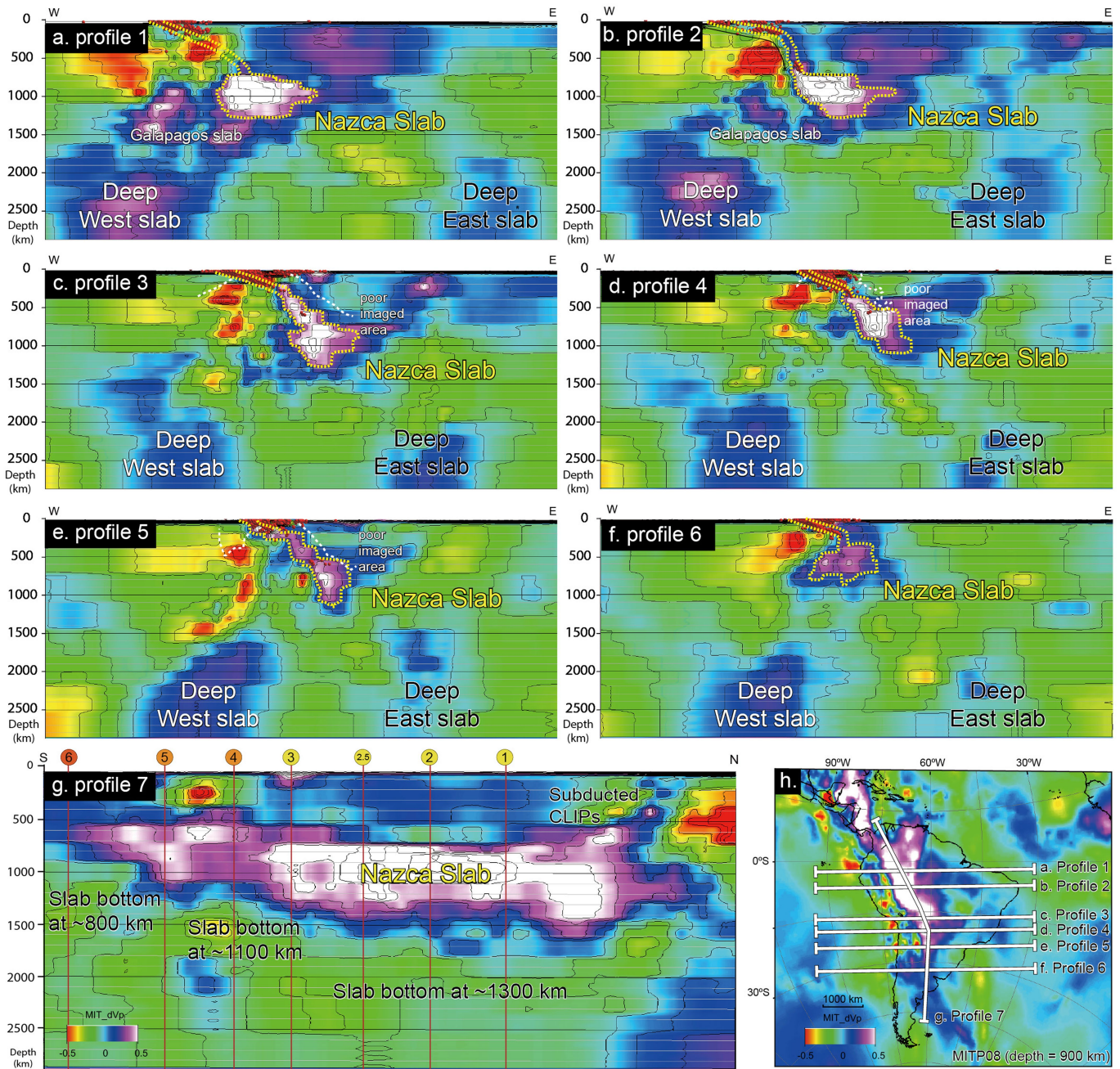
- Hafkenscheid, E., Wortel, M. J. R. & Spakman, W. Subduction history of the Tethyan region derived from seismic tomography and tectonic reconstructions. *J. Geophys. Res. Solid Earth* **111**, B08401 (2006).
- Dziewonski, A. M. & Anderson, D. L. Preliminary reference Earth model. *Phys. Earth Planet. Inter.* **25**, 297–356 (1981).
- Li, C. *Evolution of Upper Mantle Beneath East Asia and the Tibetan Plateau from P-wave Tomography*. PhD thesis, Massachusetts Institute of Technology (2007).
- Aguirre, L. & Offler, R. in *Magmatism at a plate edge: the Peruvian margin* (eds Pitcher, W. S. et al.) 59–71 (Springer, New York, 1985).
- Mukasa, S. B. Zircon U–Pb ages of super-units in the Coastal batholith, Peru: implications for magmatic and tectonic processes. *Geol. Soc. Am. Bull.* **97**, 241–254 (1986).
- Demouy, S. et al. Spatial and temporal evolution of Liassic to Paleocene arc activity in southern Peru unraveled by zircon U–Pb and Hf in-situ data on plutonic rocks. *Lithos* **155**, 183–200 (2012).
- Jones, R. E. et al. Geodynamic controls on the contamination of Cenozoic arc magmas in the southern Central Andes: insights from the O and Hf isotopic composition of zircon. *Geochim. Cosmochim. Acta* **164**, 386–402 (2015).
- Parada, M. A. et al. in *The Geology of Chile* (eds Moreno, T. & Gibbons, W.) 115–146 (Geological Society of London, London, 2007).
- Di Giulio, A. et al. Detrital zircon provenance from the Neuquén basin (south-central Andes): Cretaceous geodynamic evolution and sedimentary response in a retroarc-foreland basin. *Geology* **40**, 559–562 (2012).
- Munizaga, F. et al. Geochronology of the lake region of south-central Chile (39°–42° S): preliminary results. *J. S. Am. Earth Sci.* **1**, 309–316 (1988).
- Aragón, E., Castro, A., Díaz-Alvarado, J. & Liu, D. Y. The North Patagonian batholith at Paso Puyehue (Argentina-Chile). SHRIMP ages and compositional features. *J. S. Am. Earth Sci.* **32**, 547–554 (2011).
- Pankhurst, R. J., Weaver, S. D., Herve, F. & Larrondo, P. Mesozoic–Cenozoic evolution of the North Patagonian Batholith in Aysen, southern Chile. *J. Geol. Soc. Lond.* **156**, 673–694 (1999).
- Bissig, T., Ullrich, T. D., Tosdal, R. M., Friedman, R. & Ebert, S. The time-space distribution of Eocene to Miocene magmatism in the central Peruvian polymetallic province and its metallogenic implications. *J. S. Am. Earth Sci.* **26**, 16–35 (2008).
- Mamani, M., Wörner, G. & Sempere, T. Geochemical variations in igneous rocks of the central Andean orocline (13° S to 18° S): Tracing crustal thickening and magma generation through time and space. *Geol. Soc. Am. Bull.* **122**, 162–182 (2010).

67. Boekhout, F. et al. Mesozoic arc magmatism along the southern Peruvian margin during Gondwana breakup and dispersal. *Lithos* **146–147**, 48–64 (2012).
68. Stern, C. R. Active Andean volcanism: its geologic and tectonic setting. *Rev. Geol. Chile* **31**, 161–206 (2004).
69. Kay, S. M., Burns, W. M., Copeland, P. & Mancilla, O. in *Evolution of an Andean Margin: A Tectonic and Magmatic View from the Andes to the Neuquén Basin (35°–39°S lat)* (eds Kay, S. M. & Ramos, V. A.) 19–60 (Geological Society of America, Boulder, 2006).
70. Hervé, F., Pankhurst, R. J., Fanning, C. M., Calderón, M. & Yaxley, G. M. The South Patagonian batholith: 150 my of granite magmatism on a plate margin. *Lithos* **97**, 373–394 (2007).
71. Pilger, R. *Radiometric Dates from the Andes - Pentecost 2018 - Link* (2018).
72. Fukao, Y. & Obayashi, M. Subducted slabs stagnant above, penetrating through, and trapped below the 660 km discontinuity. *J. Geophys. Res. Solid Earth* **118**, 5920–5938 (2013).
73. Amaru, M. *Global Travel Time Tomography with 3-D Reference Models* PhD thesis, Utrecht University (2007).
74. Simmons, N. A., Myers, S. C., Johannesson, G. & Matzel, E. LLNL-G3Dv3: global P wave tomography model for improved regional and teleseismic travel time prediction. *J. Geophys. Res. Solid Earth* **117**, B10302 (2012).
75. French, S. & Romanowicz, B. Whole-mantle radially anisotropic shear velocity structure from spectral-element waveform tomography. *Geophys. J. Int.* **199**, 1303–1327 (2014).
76. Grand, S. P. Mantle shear-wave tomography and the fate of subducted slabs. *Philos. Trans. R. Soc. Lond. A* **360**, 2475–2491 (2002).
77. Hosseini, K. et al. SubMachine: web-based tools for exploring seismic tomography and other models of Earth's deep interior. *Geochem. Geophys. Geosyst.* **19**, 1464–1483 (2018).
78. Simmons, N. A., Forte, A. M., Boschi, L. & Grand, S. P. GyPSuM: a joint tomographic model of mantle density and seismic wave speeds. *J. Geophys. Res. Solid Earth* **115**, (2010).
79. Houser, C., Masters, G., Shearer, P. & Laske, G. Shear and compressional velocity models of the mantle from cluster analysis of long-period waveforms. *Geophys. J. Int.* **174**, 195–212 (2008).
80. Montelli, R., Nolet, G., Dahlen, F. A. & Masters, G. A catalogue of deep mantle plumes: new results from finite-frequency tomography. *Geochem. Geophys. Geosyst.* **7**, Q11007 (2006).
81. Koelemeijer, P., Ritsema, J., Deuss, A. & van Heijst, H. J. SP12RTS: a degree-12 model of shear- and compressional-wave velocity for Earth's mantle. *Geophys. J. Int.* **204**, 1024–1039 (2016).
82. Tesoniero, A., Auer, L., Boschi, L. & Cammarano, F. Hydration of marginal basins and compositional variations within the continental lithospheric mantle inferred from a new global model of shear and compressional velocity. *J. Geophys. Res. Solid Earth* **120**, 7789–7813 (2015).
83. Moulik, P. & Ekström, G. An anisotropic shear velocity model of the Earth's mantle using normal modes, body waves, surface waves and long-period waveforms. *Geophys. J. Int.* **199**, 1713–1738 (2014).
84. Ritsema, J., Deuss, A., van Heijst, H. J. & Woodhouse, J. H. S40RTS: a degree-40 shear-velocity model for the mantle from new Rayleigh wave dispersion, teleseismic traveltime and normal-mode splitting function measurements. *Geophys. J. Int.* **184**, 1223–1236 (2011).
85. Auer, L., Boschi, L., Becker, T. W., Nissen-Meyer, T. & Giardini, D. Savani: a variable resolution whole-mantle model of anisotropic shear velocity variations based on multiple data sets. *J. Geophys. Res. Solid Earth* **119**, 3006–3034 (2014).
86. Panning, M. P., Lekić, V. & Romanowicz, B. A. Importance of crustal corrections in the development of a new global model of radial anisotropy. *J. Geophys. Res. Solid Earth* **115**, (2010).
87. Durand, S., Debayle, E., Ricard, Y., Zaro, C. & Lambotte, S. Confirmation of a change in the global shear velocity pattern at around 1000 km depth. *Geophys. J. Int.* **211**, 1628–1639 (2017).
88. Torsvik, T. H., Müller, R. D., Van der Voo, R., Steinberger, B. & Gaina, C. Global plate motion frames: toward a unified model. *Rev. Geophys.* **46**, RG3004 (2008).
89. O'Neill, C., Müller, D. & Steinberger, B. On the uncertainties in hot spot reconstructions and the significance of moving hot spot reference frames. *Geochem. Geophys. Geosyst.* **6**, Q04003 (2005).
90. Butterworth, N. P. et al. Geological, tomographic, kinematic and geodynamic constraints on the dynamics of sinking slabs. *J. Geodyn.* **73**, 1–13 (2014).
91. Domeier, M., Doubrovine, P. V., Torsvik, T. H., Spakman, W. & Bull, A. L. Global correlation of lower mantle structure and past subduction. *Geophys. Res. Lett.* **43**, 4945–4953 (2016).
92. Zahradník, J. et al. A recent deep earthquake doublet in light of long-term evolution of Nazca subduction. *Sci. Rep.* **7**, 45153 (2017).
93. Goes, S., Capitanio, F. A. & Morra, G. Evidence of lower-mantle slab penetration phases in plate motions. *Nature* **451**, 981–984 (2008).



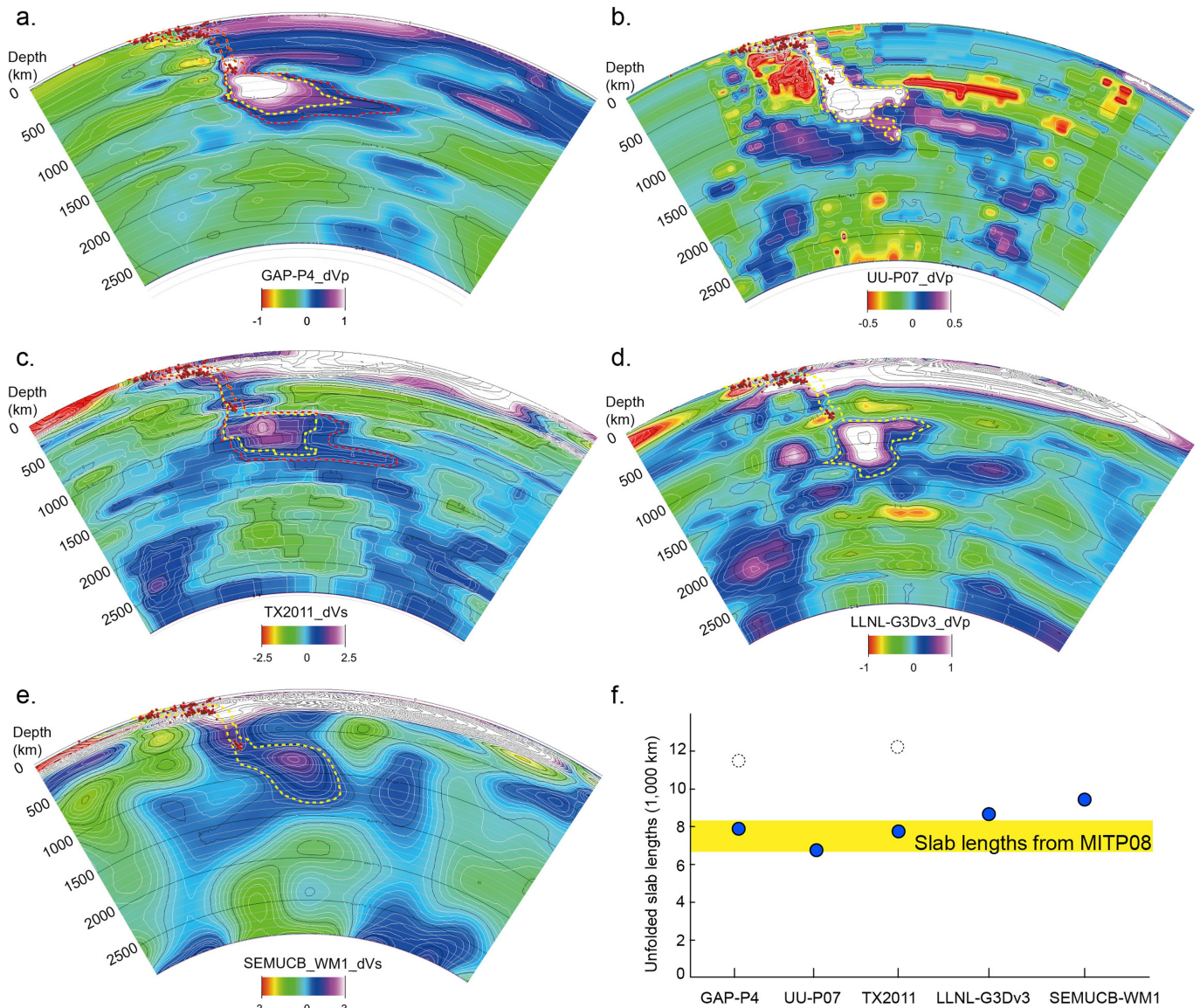
Extended Data Fig. 1 | Slab anomalies under South America. The anomalies are shown in different tomographies within a UTM (Universal Transverse Mercator) projection at 400 km (left), 1,000 km (middle) and 1,200 km (right). Tomographies include: **a.** MITP08¹⁰, **b.** GAP-P4⁷²; **c.** UU-P07⁷³; **d.** LLNL-G3Dv3⁷⁴; **e.** SEMUCB-WM1⁷⁵; and **f.** TX2011⁷⁶. dVp and dVs are the velocity perturbations (expressed as a percentage) from P-wave and S-wave tomography, respectively. **g.** Map^{26,77} of the number (out of 22) of global seismic tomography models that show

fast velocity anomalies at a given location, which gives an indication of imaging robustness. The 22 tomographies include MITP08¹⁰, GAP-P4⁷², UU-P07⁷³, LLNL-G3Dv3⁷⁴, SEMUCB-WM1⁷⁵, TX2011⁷⁶, GyPSuM⁷⁸, HMSL-P06⁷⁹, PRI-P05⁸⁰, SP12RTS-P⁸¹, SPani-P⁸², S362ANI+M⁸³, S40RTS⁸⁴, SAVANI⁸⁵, SAW642ANb⁸⁶ and SEISGLOB2⁸⁷. Overall, the northern Nazca slab shows a wider tomographic anomaly that is stronger in amplitude and extends deeper into the lower mantle relative to the southern slab.



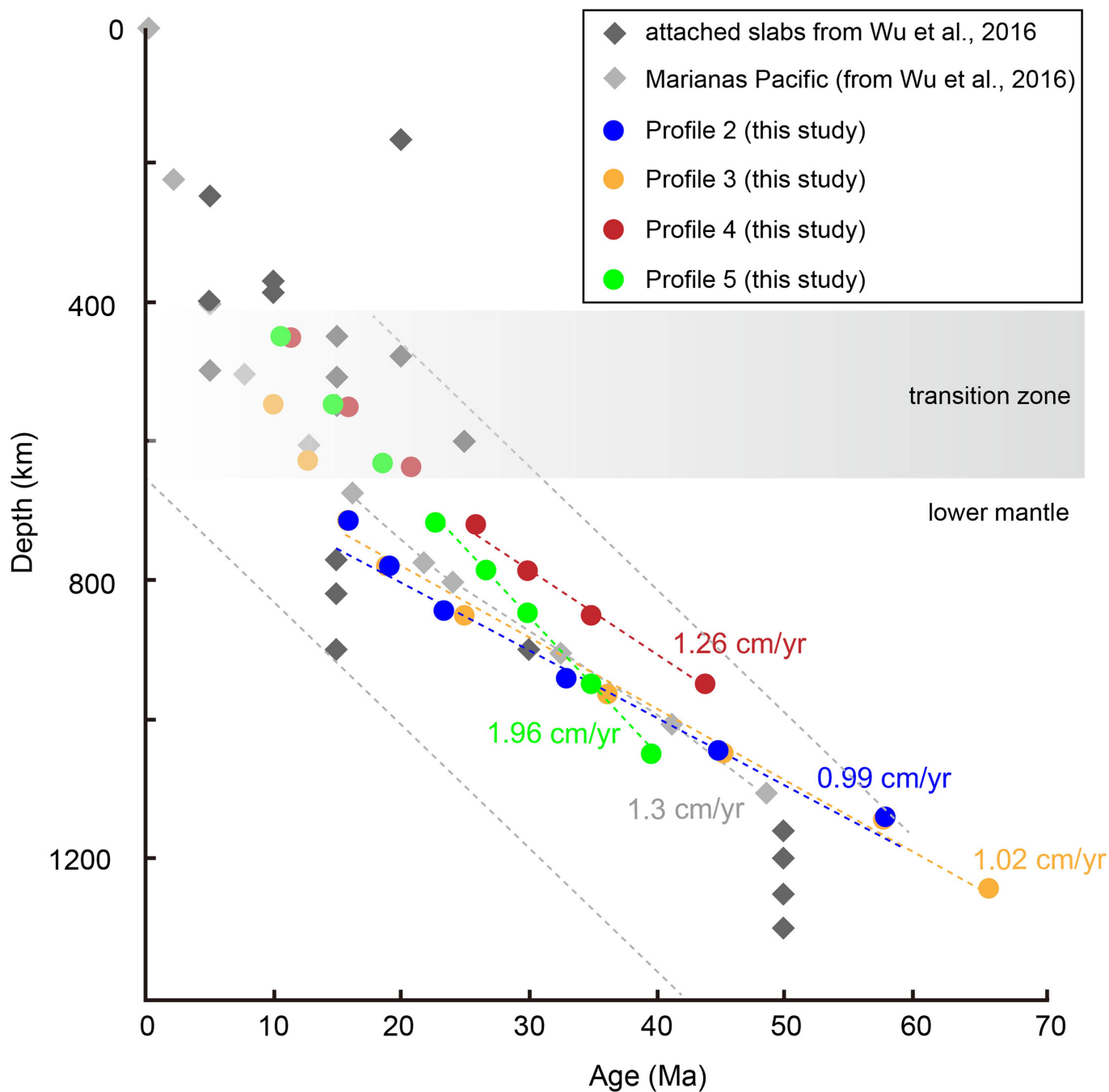
Extended Data Fig. 2 | Tomographic cross-sections showing the Nazca slab from MITP08 tomography. a–f, East–west sections (see **h**) are shown from north to south. Red dots indicate Benioff zone seismicity. Yellow dashed lines show our manually selected Nazca slab edges that were primarily defined by steep velocity gradients. Poorly imaged areas

identified by previous tomography studies are highlighted by white dashed lines^{11–13}. **g,** A trench-parallel profile. Intersections with east–west profiles 1–6 are shown by red lines. **h,** Profile positions on a horizontal slice at a depth of 900 km within a UTM projection.



Extended Data Fig. 4 | Cross-sectional area unfolding method applied to the other five tomographies at profile 2. See Extended Data Fig. 2g for location. **a**, GAP-P4⁷²; **b**, UU-P07⁷³; **c**, TX2011⁷⁶; **d**, LLNL-G3Dv3⁷⁴; and **e**, SEMUCB-WM1⁷⁵. Our choices of slab edges are shown as yellow dashed lines, with $dV_p = +0.3\%$ in UU-P07 (**b**) and LLNL-G3Dv3 (**d**), $dV_p = +0.6\%$ in GAP-P4 (**a**), $dV_s = +0.9\%$ in TX2011 (**c**) and $dV_s = +0.7\%$ in SEMUCB-WM1 (**e**). **f**, The unfolded slab lengths from

the five tomographies, with our choices of slab edges shown as blue circles. Unfolded slab lengths from MITP08 in Extended Data Fig. 3d are shown as a yellow box. The unfolded slab lengths of an alternative slab area in GAP-P4 and TX2011 (red dashed lines in **a** and **c**) are shown as open dashed circles. Overall, the slab lengths from the six tomographies show similar results.

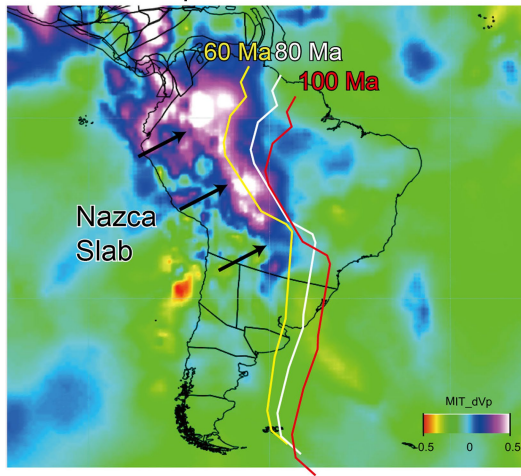


Extended Data Fig. 5 | Age–depth curve for our unfolded Nazca slab for profiles 2–5. Implied lower-mantle sinking rates are shown by the circles and labels, coloured coded by tomographic profile. For comparison, we also plot lower-mantle sinking rates at the central Marianas Pacific

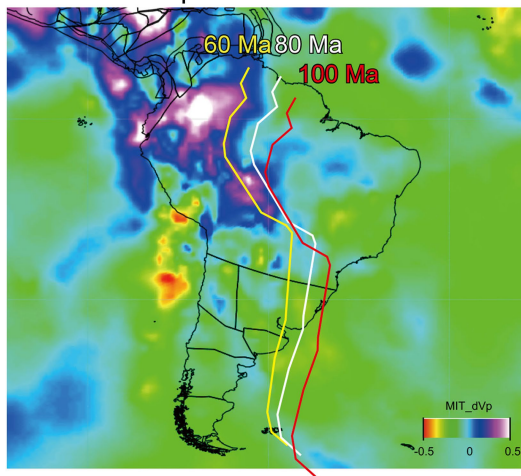
slabs (light grey diamonds)²¹ and age–depth relationships of slabs under east Asia (dark grey diamonds)²¹. All sinking rates from this study are consistent with ref. ²¹, which found an average lower-mantle sinking rate of $1.8 \pm 0.8 \text{ cm yr}^{-1}$ (grey dashed lines).

Torsvik et al. (2008)
mantle reference frame

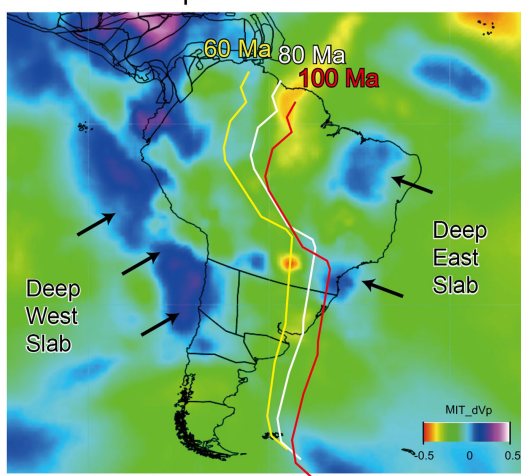
a. 1200 km depth



c. 1400 km depth

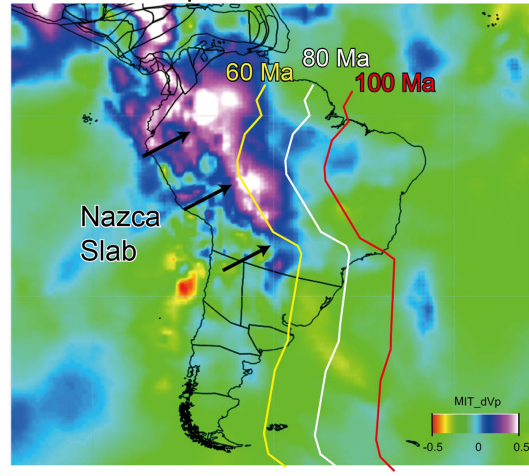


e. 1600 km depth

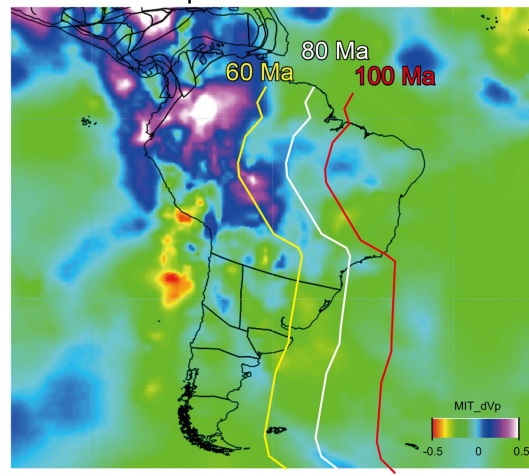


O'Neill et al. (2005)
mantle reference frame

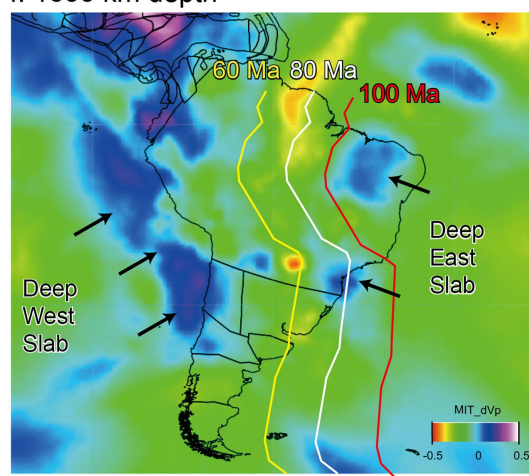
b. 1200 km depth



d. 1400 km depth

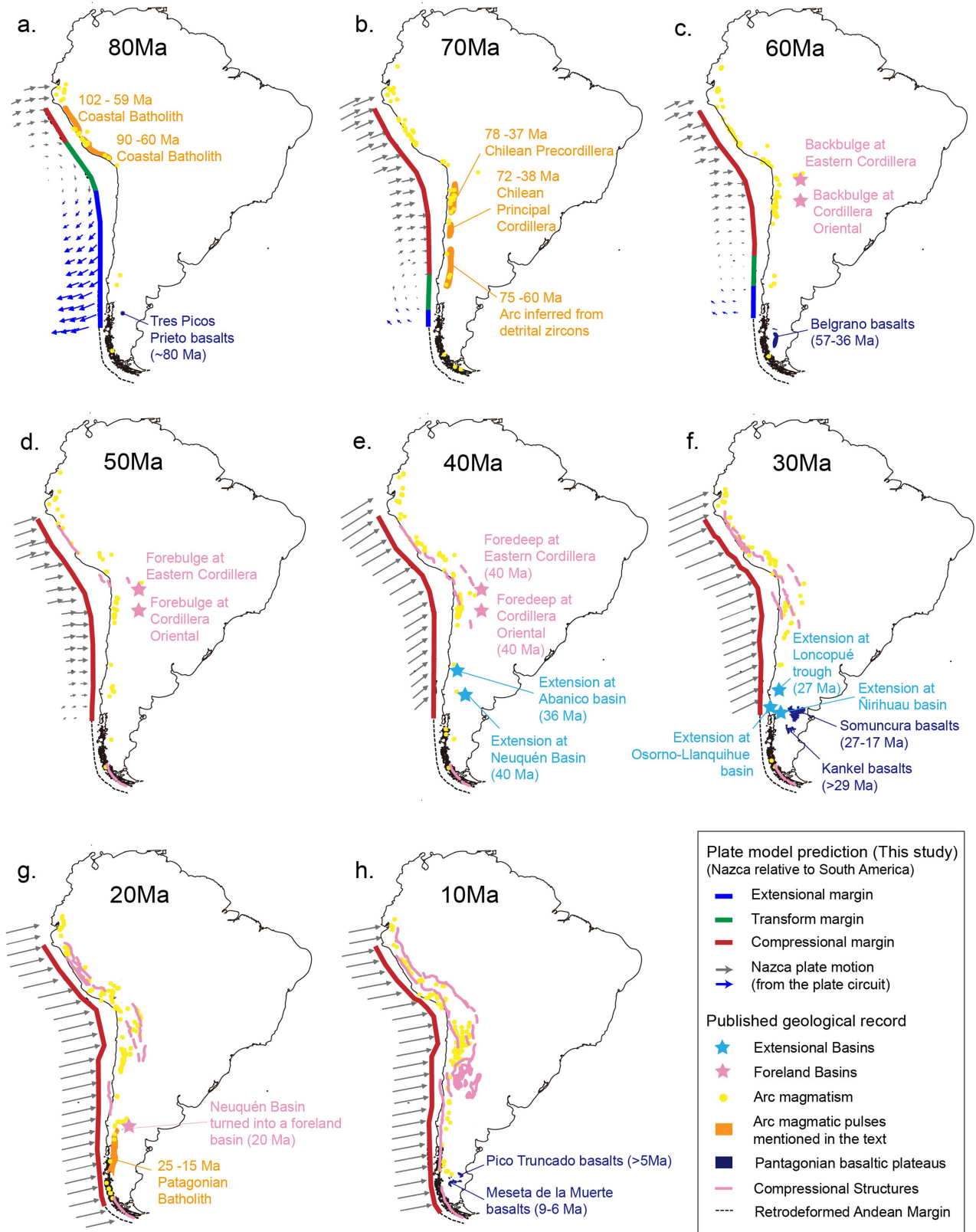


f. 1600 km depth



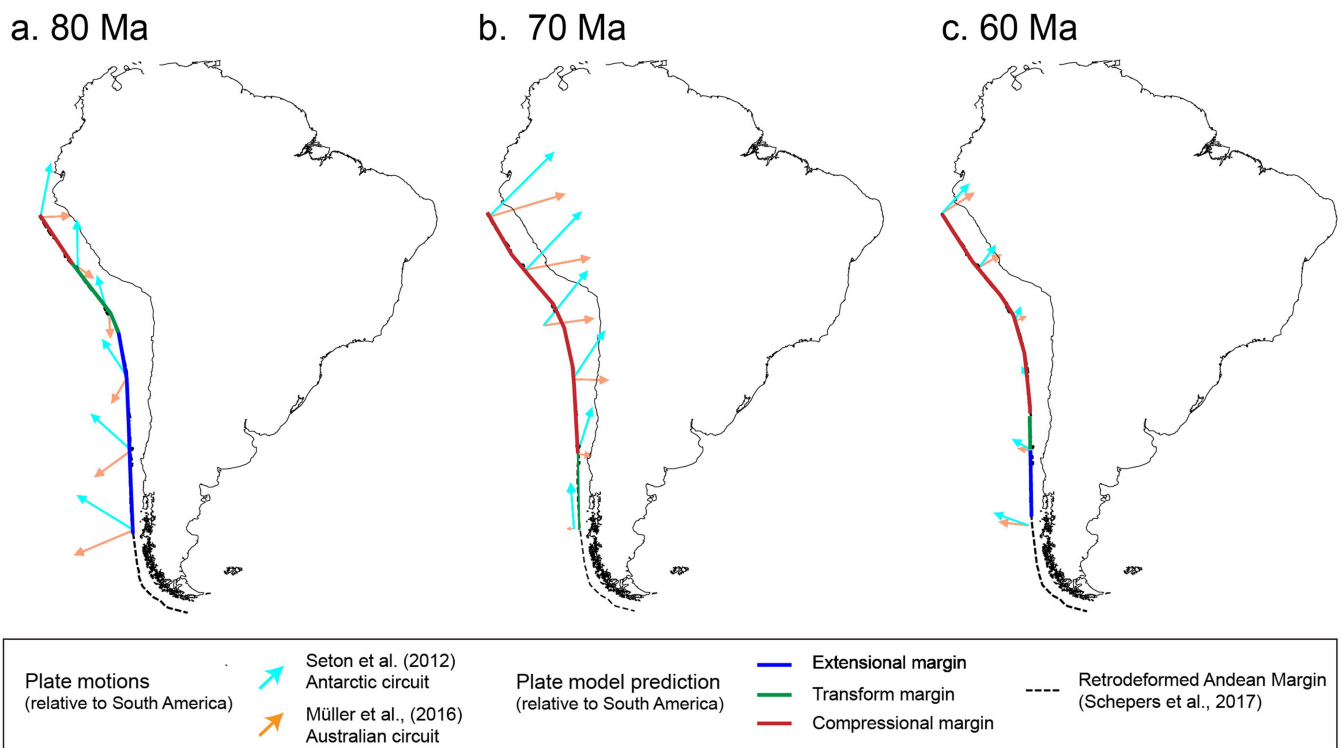
Extended Data Fig. 6 | Reconstructed Nazca trench positions between 100 Myr and 60 Myr ago within two alternative mantle reference frames. Reconstructed trench positions are shown at 100 Myr ago (red lines), 80 Myr ago (white lines) and 60 Myr ago (yellow lines), superimposed on horizontal sections of MITP08 tomography¹⁰ within

mid- to lower-mantle depths (a, b, 1,200 km; c, d, 1,400 km; e, f, 1,600 km). a, c, e, Reconstructions based on the mantle reference frame of ref. ⁸⁸. b, d, f, Reconstructions based on the mantle reference frame of ref. ⁸⁹.



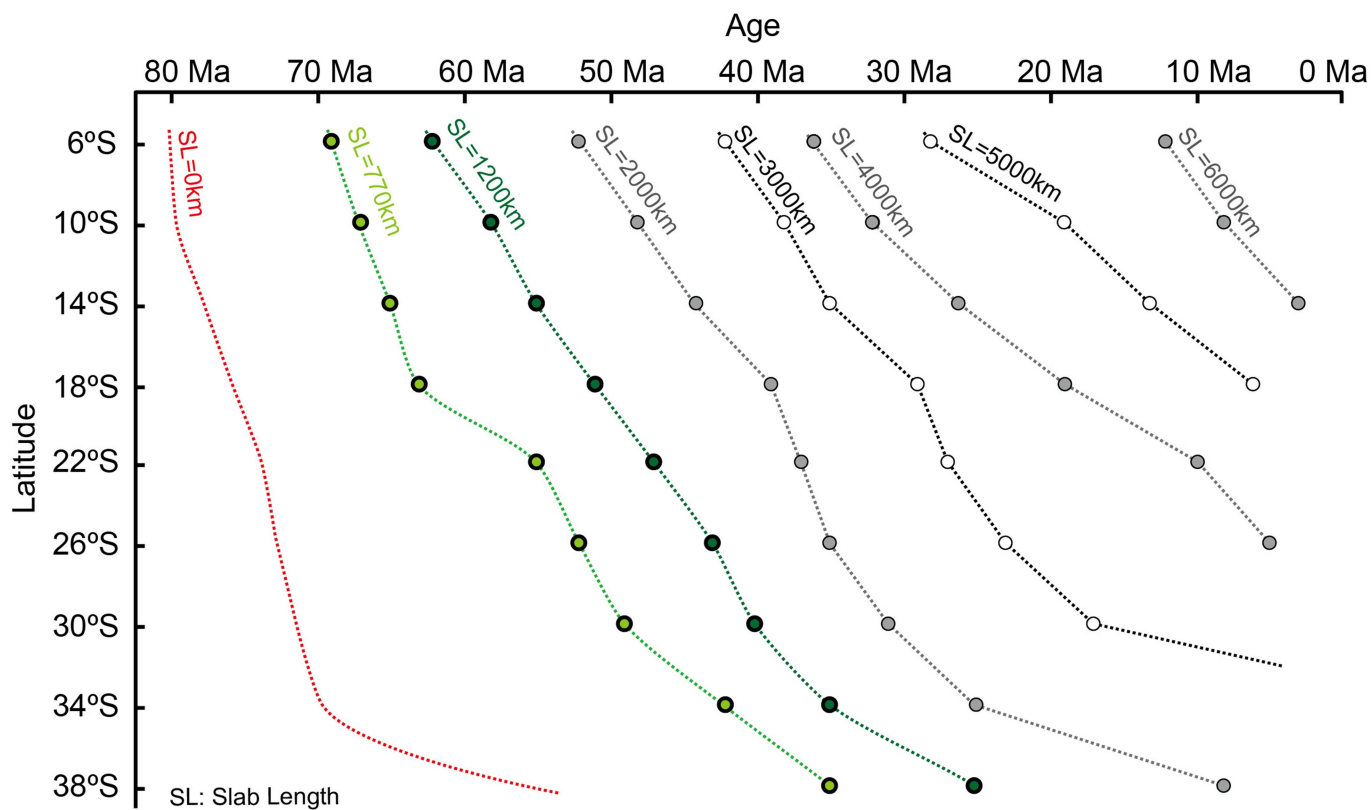
Extended Data Fig. 7 | Reconstructed Nazca plate motions relative to a fixed South America. a, 80 Myr ago; b, 70 Myr ago; c, 60 Myr ago; d, 50 Myr ago; e, 40 Myr ago; f, 30 Myr ago; g, 20 Myr ago; h, 10 Myr ago. Grey arrows indicate the motion of the subducting Nazca plate relative to South America. Divergent motions are shown by blue arrows. The position

of the Nazca–South America plate boundary is based on the retrodeformed Andean margin from ref. ²³. Subduction along the Nazca–South America plate boundary is highlighted by the thick red line; green and blue thick lines indicate transform and divergent plate boundaries, respectively. Other references are the same as in Fig. 4.



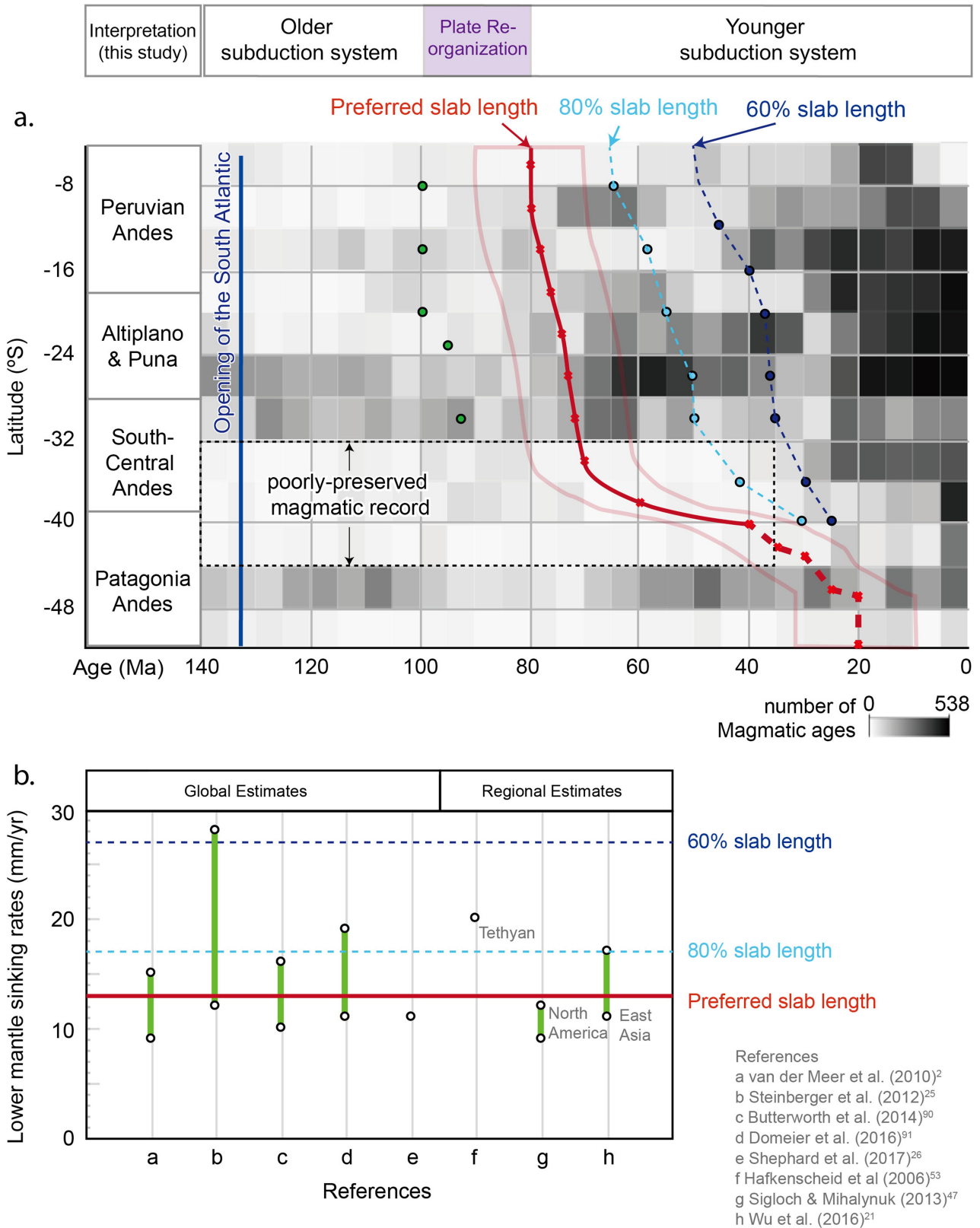
Extended Data Fig. 8 | Comparison of Nazca–South America plate motions from alternative plate circuits. **a–c**, Plate motions 80 Myr ago (**a**), 70 Myr ago (**b**) and 60 Myr ago (**c**) are shown from the Antarctic plate circuit²⁷ (blue arrows) and the Australian plate circuit³ (orange arrows). In this study, we followed the plate motion derived from the Australian plate circuit³. The Australian circuit assumes limited motion between the Lord Howe Rise and the Pacific before the Eocene. This allows a motion chain to be built from East Antarctica to Australia to the Lord Howe Rise/Pacific, avoiding the less-well-constrained relative motion of East and

West Antarctica, on which the Antarctic circuit is built (see ref.²⁹ for an in-depth discussion). Both models indicate coeval northern convergence and southern divergence, although the motions are different in the late Cretaceous (**a** and **b**). The position of the Nazca–South America plate boundary is based on the retro-deformed Andean margin (black dash lines)²³. Subduction along the plate boundary is coloured in red; green and blue indicate transform and divergent plate boundaries, respectively (same as in Extended Data Fig. 7).



Extended Data Fig. 9 | Subducted-slab lengths along the western South American margin over time. Slab lengths (SLs) are based on our plate model and measured over time between the leading edge of the subducted Nazca slab and the retro-deformed Andean margin²³. A slab length of 0 km indicates Nazca subduction initiation. A slab length of 770 km

indicates the earliest possible time that the Nazca slab could have reached the lower mantle, based on a sub-vertical Marianas slab end-member³⁰. A slab length of 1,200 km indicates the latest possible time that the Nazca slab could have reached the lower mantle, based on a shallow-dipping Peruvian flat-slab end-member³⁰. See main text for more details.



Extended Data Fig. 10 | See next page for caption.

Extended Data Fig. 10 | Sensitivity of our plate model to other possible slab lengths and their implied sinking rates. a, Our plate model predictions are compared with a spatial density plot of total recorded Andean magmatic ages by latitude from a catalogue of undifferentiated Andean magmatic ages⁷¹ (14,709 total published magmatic ages since 140 Myr ago). The bin size is 4° in latitude and 5 Myr in age. This plot is designed to offer an alternative perspective to Fig. 5a. Differences between this plot and Fig. 5a result from our choice of including in Fig. 5a only magmatism that had an interpreted tectonic origin, for example, arc-related, backarc or intraplate magmatism. For Fig. 5a, published geochemical signatures provide a feature-by-feature comparison for each magmatic record that is absent from this plot. The near-white band 32° S and 45° S is not necessarily a magmatic gap, but is the result of limited reported ages, possibly owing to limited outcrop exposure. In Fig. 5a, we used detrital zircon ages to infer the magmatic activity for 32°–45° S. The thick red line shows our predicted southward propagation of Nazca subduction initiation (same as in Fig. 5a). The error range (± 10 Myr) shown by transparent red lines come from alternative choices of slab-edge velocity perturbations (see Methods and Extended Data Fig. 3 for details). Overall, our model prediction fits well with a magmatic minimum around

80 Myr ago followed by increased magmatism, which we interpret to correspond to the initiation of the most recent phase of Nazca subduction. Arbitrarily decreased unfolded slab lengths of 80% (light blue dashed line) and 60% (dark blue dashed line) are also shown. The arbitrarily decreased slab lengths show the sensitivity of our plate model predictions to possible tomographic blurring, which would have exaggerated our measured Nazca slab areas. Comparison to the shorter unfolded slab lengths shows that southward propagation of Nazca subduction is preserved when Nazca slab lengths are decreased, but we argue that the alternative subduction initiation timings compare less well to the increased magmatism between 80 Myr and 60 Myr ago north of 32° S. Green dots show that the choice of a thinner initial lithosphere thickness for slab unfolding (80 km rather than 100 km) would increase slab lengths, which would effectively offset some tomographic blurring. **b,** Comparison between published lower-mantle slab sinking rates^{2,21,25,26,47,53,90,91} and the implied lower-mantle sinking rates for our preferred slab lengths (red line) and arbitrarily decreased 80% (light blue dashed line) and 60% (dark blue dashed line) slab lengths from **a**. Shorter slab lengths (less than 60%) were excluded from **a** on the basis of unreasonably fast slab sinking rates.

Extended Data Table 1 | Notable ages of Nazca subduction

Reference	Latitude	Age of subduction Initiation	Time that slab reached 660 km depth	Earliest time of slab penetration below 660 km depth	Method
This study	~6°S	~80 ±10 Ma	69-62 Ma	69 Ma	Cross-sectional area unfolding from MITP tomography ¹⁰
	~10°S	~80 ±10 Ma	67-58 Ma	67 Ma	
	~14°S	~78 ±10 Ma	65-55Ma	65Ma	
	~18°S	~76 ±10 Ma	63-51 Ma	63 Ma	
	~22°S	~74 ±10 Ma	55-47 Ma	55 Ma	
	~ 26 °S	~73 ±10 Ma	52-43 Ma	52 Ma	
	~30°S	~72 ±10 Ma	49-40 Ma	52 Ma	
	~34°S	~70 ±10 Ma	42-35 Ma	42 Ma	
	~38°S	~55 ±10 Ma	35-28 Ma	35 Ma	
Grand ¹⁴	~6°N -30°S	~50 Ma	NA	NA	Estimated slab lengths from V _s tomography ¹⁴
Ren, <i>et al.</i> ¹⁵	~6°N-12°S	~50 Ma	NA	NA	Estimated slab lengths from V _s tomography ¹⁵
Faccenna, <i>et al.</i> ⁸	~20°S	~60 Ma	NA	~50±10 Ma	Numerical modeling
Quinteros and Sobolev ¹⁶	~20°S	25-20 Ma [†]	NA	16-10 Ma [†]	Numerical modeling
Zahradník, <i>et al.</i> ⁹²	~6°N-12°S	~110 Ma [†]	NA	~68 Ma [†]	Numerical modeling
Schellart ⁹	The whole margin	NA	~167-152 Ma	~132.5-80 Ma	Numerical modeling
Goes, <i>et al.</i> ⁹³	Columbia to Peru	NA	NA	40-50 Ma	Plate advance and trench retreat rates
Mpodozis and Ramos ¹	The whole margin	~190 Ma	NA	NA	Geology

We provide our proposed times for the initiation of Nazca subduction, for the Nazca slab reaching the lower mantle (660 km depth) and for its penetration into lower mantle, along with those determined in published studies^{1,8,9,14-16,92,93}. NA, not available.

[†]The original geodynamic models were forward models that began at 0 Myr ago. Time periods have been adjusted for comparison.